Quaternary Science Reviews 205 (2019) 193–223

Contents lists available at ScienceDirect

Quaternary Science Reviews

journal homepage: www.elsevier.com/locate/quascirev

Anatomy of a late Quaternary carbonate island: Constraints on timing and magnitude of sea-level fluctuations, West Caicos, Turks and Caicos Islands, BWI

Charles Kerans [a, *], Chris Zahm [b], Steven L. Bachtel [c], Paul Hearty [d], Hai Cheng [e, f]

[a] Department of Geological Sciences, and Bureau of Economic Geology, Jackson School of Geosciences, The University of Texas at Austin, USA
[b] Bureau of Economic Geology, Jackson School of Geosciences, The University of Texas at Austin, USA
[c] Department of Geological Sciences, Jackson School of Geosciences, The University of Texas at Austin, formerly of Chevron Energy Technology Company, Houston, USA
[d] Department of Geological Sciences, Jackson School of Geosciences, The University of Texas at Austin, USA
[e] Institute of Global Environmental Change, Xi'an Jiaotong University, Xi'an, 710049, China
[f] Department of Earth Sciences, University of Minnesota, Minneapolis, 55455, USA

ARTICLE INFO

Article history:
Received 4 August 2018
Received in revised form
26 November 2018
Accepted 7 December 2018
Available online 28 December 2018

ABSTRACT

The data set of the island of West Caicos consists of a combination of high-resolution lidar and digital imagery, radiometric data, and amino acid racemization (AAR) D/L values as well as extraordinary preservation of sedimentary and bio-constructed deposits on the island. Together with a well-established regional stratigraphic framework from the neighboring Bahamian island chain and detailed field mapping, the West Caicos data set provides an opportunity to advance our understanding of the link between carbonate stratigraphy and the controlling parameters of sea level, sediment supply, tectonics, and climate. The exceptionally well-preserved stratigraphic record of the mid–late Pleistocene from West Caicos allows recognition of marine isotope stages (MIS) 9/11, 5e, and Holocene. The west coast of the island provides a continuous 8.4 km exposure of the MIS 5e record that enhances our understanding of the intra-MIS 5e bipartite succession in this region and supports a sea-level lowering that occurred during the last interglacial (LIG).

West Caicos accreted as a series of eolian, foreshore–shoreface, barrier-reef, and fringing-reef facies. Shoreline positions for all but the MIS 7 and MIS 5a/c deposits are now captured in the sub-meter geodetic-quality topobathy lidar survey. The Star Town unit of MIS 9/11 age forms the southern margin of the island as well as the central karst-modified spine, with uranium–thorium (U–Th) coral ages of between 368 and 365 thousand years ago (ka) and a D/L Glu average of >0.60. Early MIS 5e strata include the Railroad Ridge unit in the center of the island, which was previously identified as one of the older units. The Railroad Ridge unit is a north–south linear dune ridge that has a D/L Glu average of 0.52 and indicates the onset of sediment sources from the east associated with a flooded central Caicos Platform. Approximately synchronously, the early MIS 5e South Reef unit (+3.75–4 m sea-level elevation) nucleated on the western coast of West Caicos, attached to the middle Pleistocene Star Town unit. The South Reef corals yield an average coral U–Th age of **126.5 ka**, with an average D/L Glu from skeletal matrix of 0.46. This transitional barrier/fringing reef is unconformably overlain by the late MIS 5e Boat Cove unit. Corals in the basal transgressive phase of this *upper* MIS 5e Boat Cove unit yield an average **120.6 ka** U–Th and average D/L Glu of 0.45. Shallow-marine, foreshore, and eolian facies of the late MIS 5e rest on a wave-cut terrace that cuts the early MIS 5e South Reef unit by as much as 3 m down to a +0.5 m above present sea-level elevation. The upper MIS 5e Boat Cove unit displays a maximum of +4.5 m elevation above present-day sea level, measured from the middle of the foreshore. This estimate may be a minimum value as the exposures on the west coast are part of a forced regressive foreshore sequence. Last stages of the upper MIS 5e deposition are seen in a series of regressive dune-beach ridge deposits referred to as the Northeast Ridges unit, with sea-level positions ranging from +4.5 m early in the central part of West Caicos, to +0.5 m on the far northeast coast, eventually building down below present-day sea level. This sea-level history fits well with previously documented

* Corresponding author.
E-mail address: ckerans@jsg.utexas.edu (C. Kerans).

https://doi.org/10.1016/j.quascirev.2018.12.010
0277-3791/

records in the Bahamas and globally, and the extensive erosion supports a short-lived (between 126 and 120 ka) intra-MIS 5e relative-sea-level fall. Holocene deposition on West Caicos is restricted to northern and eastern margins of the island as a combination of strandplain and dune ridge mixed skeletal–oolitic units.

Using the high-resolution digital elevation model (DEM) and linked digital geologic map makes it possible to compare areas of the different Pleistocene and Holocene units quantitatively and to constrain volumetric assessments and accumulation rates on the island for different units. The peak sediment volume production/accumulation rate—between 6.5 and 8×10^6 m^3 or between 2.2 and 2.7×10^6 m^3 per ka—is observed in the upper MIS 5e unit. This rate is 5 times greater than the 0.5×10^6 m^3 per ka estimated for the Holocene ooid dune-ridge/strandplain complex, suggesting that the combination of higher sea level, greater wave and wind energy, and warmer ocean temperatures may have fostered the higher rate of chemically precipitated sediment supply.

1. Introduction

The mid–late Pleistocene carbonates of the greater Bahamas–Turks and Caicos (BTC) island chain in the western North Atlantic provide unique constraints on the depositional and diagenetic history of shallow-water carbonate cycles of icehouse Milankovitch affinity (Figs. 1 and 2) (cf. Read, 1999). These islands have also assumed a central role in the debate about global warming and climate changes as they contain one of the highest resolution records of past climate and sea-level during the most recent period of Earth history, when temperatures were higher than today and sea-level was between +6 and + 9 m above present mean datum. Extensive work has been carried out on the stratigraphy, geochronology, and sea-level history of these islands, but if one considers their importance in understanding past peak interglacial periods and high sea levels, their stature pales when compared to the extensive work in polar regions. This current effort seeks to add to our knowledge of these important BTC records, at the same time pointing to the huge potential for a new generation of studies of these islands that will integrate lidar and unmanned aerial vehicle (UAV) data along with new high-resolution age dating to further enhance and elucidate our view of these ancient paleo-environmental archives.

Although outcropping BTC limestones are volumetrically dominated by eolian dune-ridge deposits and classified as eolian islands by Vacher and Quinn (1997), a spectrum of shoreface, foreshore, washover, reef, and lagoon/salina environments can provide a detailed record of sea level during the short but critical peak interglacial highstands driven by climatic thermal maxima. Where detailed sedimentologic/stratigraphic studies have been coupled with absolute and/or relative age constraints from U–Th radiometric dating and amino acid racemization (AAR), it has been possible to provide important bounds on the magnitude and timing of sea level during peak warming (Chen et al., 1991; Hearty and Kindler, 1993; Carew and Mylroie, 1985, 1995; Kindler and Hearty, 1996; Hearty, 1998; Blanchon et al., 2009; Muhs et al., 2011). However, only a handful of the more-than-700 Bahamian islands have been analyzed in detail, and even frameworks from islands

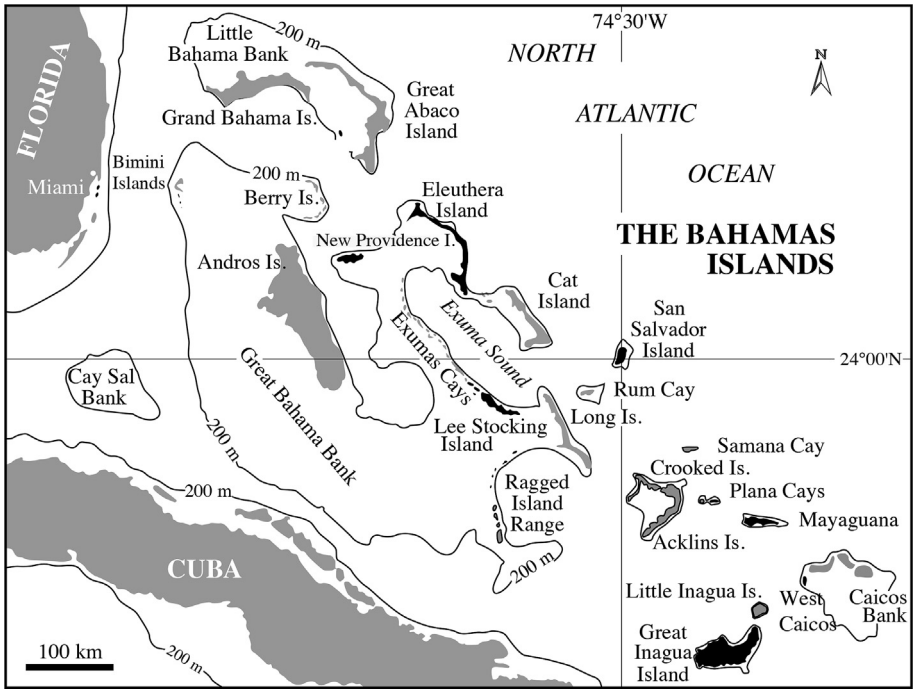

Fig. 1. Western North Atlantic BTC platforms and related carbonate platforms. Islands with detailed age dates and sea-level documentation are highlighted. Modified from Hearty and Kaufman (2009).

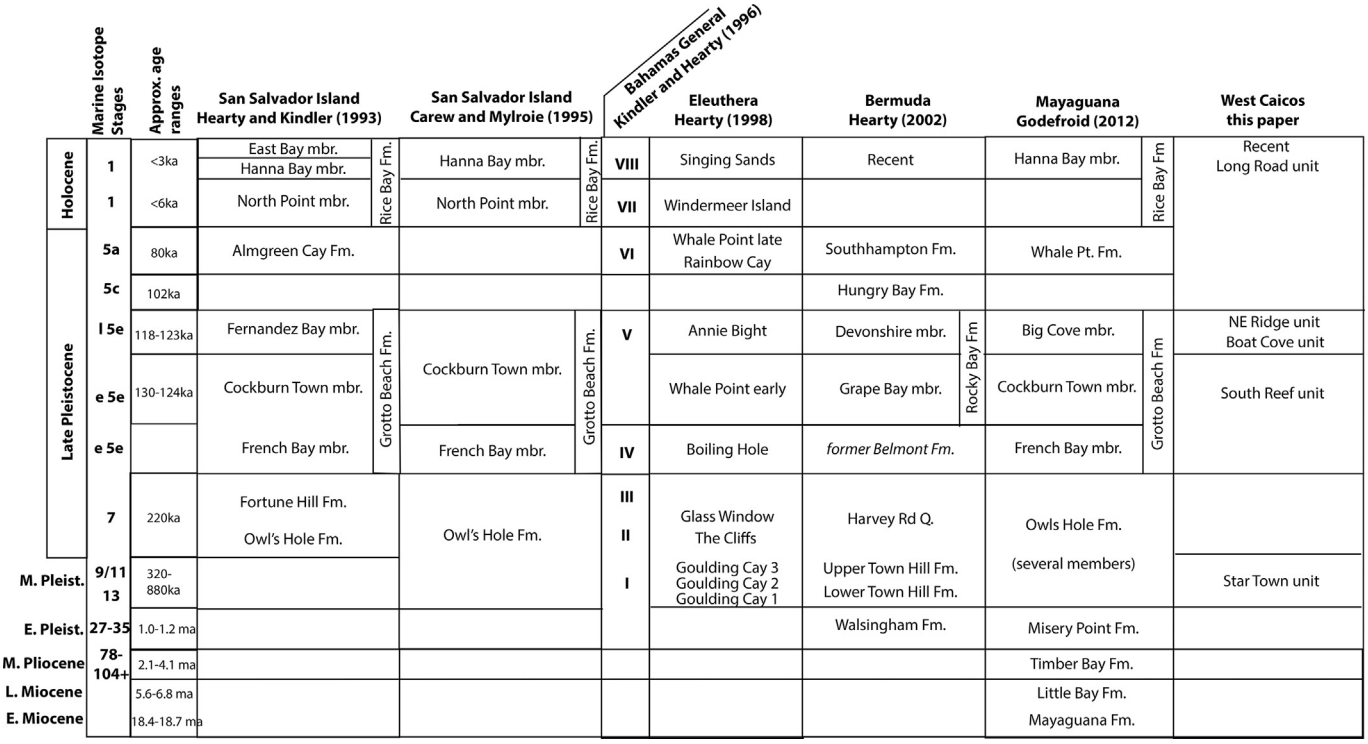

Fig. 2. Stratigraphic chart illustrating stratigraphic frameworks from several key Pleistocene exposures in the Bahamas/West Indies region.

such as Eleuthera and New Providence, where much of the type stratigraphic work has been documented, may be in a state of change. Major changes in technology, in particular the advent of high-resolution DEMs from airborne lidar and UAVs, are now providing an unparalleled ability to unravel the three-dimensionally complex icehouse record of these exposures.

How much additional information can be gleaned from these critical control points when interrogating these exposures with available technologies, combined with traditional field mapping and the stratigraphic models already developed from the region? West Caicos provides an ideal opportunity to investigate the upside potential of the application of these new instruments, combined with fieldwork and geochronology, to develop a high-resolution island stratigraphy and sea-level history. West Caicos is a typical leeward island (type IV of Kindler and Hearty, 1997) in the BTC that has received a substantial amount of previous carbonate facies and depositional-systems analysis (Waltz, 1988; Wanless and Dravis, 1989; Guidry et al., 2007; Simo et al., 2008; Kindler and Meyer, 2012), but a rigorous Pleistocene stratigraphic framework has yet to be provided. Whereas many of the islands such as Bermuda, New Providence, San Salvador, and Eleuthera have gone through multiple iterations to reach the current high level of resolution of the Pleistocene framework and quantified sea-level history, we have attempted to compress that cycle time by leveraging digital-mapping technologies together with detailed field mapping, AAR and U–Th dating, and past experience from neighboring islands. Clearly if cycle time for developing island stratigraphic frameworks can be substantially reduced and spatial resolution improved, the potential exists to further elaborate the complex temporal and chronologic record of sea-level change across this suite of BTC stratigraphic data points. In turn, the greater spatial–temporal resolution of sea-level position will aid our understanding of interglacial sea-level dynamics and also help to further constrain models of glacio-isostatic adjustments across the region.

Bare-earth imagery from airborne lidar data (Kraus and Pfeifer, 1998; Haugerud and Harding, 2001) is extremely well suited to the morphostratigraphic approach advocated for many of the Bahamian islands (Vacher, 1973; Garrett and Gould, 1984; Hearty and Kindler, 1993; Kindler and Hearty, 1997). The importance of elucidating the geomorphology of these islands through the heavy overgrowth with lidar-generated bare-earth models cannot be underestimated. These models allow the geologist to extend investigations from the wave-cut coasts across the full island interior, enabling high-resolution mapping across the entire surface area as well as clearly revealing relative age relationships through features such as unit-specific karst development. Quantitative DEMs also afford the opportunity to analyze for unit-specific sediment volumes and thus sedimentation rates. These rates will allow a new quantitative level of interrogation of interglacial sequence evolution and possibly point to important trends in temperature or geochemical controls on carbonate factories through time. Finally, we will highlight here the utility of UAV-acquired photography and structure from motion (SfM) mapping (Turner et al., 2012; Westoby et al., 2012), which have proven to be useful in many other geologic applications (e.g., Zahm et al., 2016). The ability to capture high-resolution depositional facies patterns and improve 3D facies architectural analysis is ideally suited for many coastal exposures such as we will show on West Caicos.

The goal of this study is to generate a high-quality geologic model of a typical leeward BTC island by leveraging existing understanding of Bahamian Pleistocene stratigraphy and newly available remote-imagery technology, together with high-resolution stratigraphic mapping. In doing so, we have added a robust stratigraphic record of the last 400 ky of Pleistocene stratigraphy and have developed what should be considered one of the best constrained intra-MIS 5e geologic frameworks currently available for the region.

2. Bahamian Pleistocene framework: previous work

Detailed studies of western North Atlantic Pleistocene carbonate-island stratigraphy have provided a framework that is finely tuned to the short-lived highstand portion of the high-amplitude, high-frequency, eccentricity-driven sea-level signal as well as to sub-Milankovitch events (Fig. 3). This glacioeustatic forcing during the mid–late Pleistocene is superimposed on relatively stable tectonic terrain in the Bahamas and through the Turks and Caicos platform (2 cm/ka) (Lynts, 1970; Mullins and Lynts, 1977; Freeman-Lynde and Ryan, 1985). It should be noted that these subsidence estimates derive from Cenozoic through present stratigraphic sections and that the subsidence record since MIS 5e represents only 0.1 percent of this time-averaged period (Hearty, 1998), and thus any generalizations of vertical motion need to be made with caution.

Island studies of New Providence (Garrett and Gould, 1984; Hearty and Kindler, 1997), San Salvador (Carew and Mylroie, 1985, 1995; Chen et al., 1991; Hearty and Kindler, 1993), Eleuthera (Kindler and Hearty, 1995; Hearty, 1998), Lee Stocking (Kindler, 1995), Mayaguana (Kindler et al., 2011; Godefroid, 2012), Crooked (Godefroid and Kindler, 2016) and the Turks and Caicos (Wanless and Dravis, 1989; Simo et al., 2008; Kindler and Meyer, 2012) have established a broad framework that includes multiple formation and member-level units of the mid-Pleistocene–Holocene (Fig. 2). An overview of Bahamian archipelago studies generally demonstrates the commonality of morphostratigraphic sequences and chronologies among most islands (Kindler and Hearty, 1996; Hearty and Kaufman, 2000). The record on Eleuthera (Kindler and Hearty, 1996, 1997; Hearty, 1998) captures the most detailed through-going framework, with three main highstands (MIS 1–Holocene, MIS 5e–Eemian or LIG, and MIS 9/11) as well as MIS 5a and MIS 7 aeolianites. As in Bermuda, there are some remnant, relic, older middle and early Pleistocene rocks in the Bahamas (e.g. Godefroid, 2012; Godefroid and Kindler, 2016), but the majority of evidence points to initiation of major island building over the past half million years.

Both Bahamian and global studies of the widespread MIS 5e record (Hearty et al., 2007) have drawn attention to sub-Milankovitch-scale eustatic forcing and stratigraphic responses that could easily have been overlooked in the older rock record. A six-stage sea-level pattern—including a rise to +3–4 m followed by a fall to the present datum and a subsequent rise to +6 m before the steady downstepping of the MIS 5d-c—has been proposed for New Providence, Eleuthera, San Salvador, Abaco, and Exumas Islands (Hearty et al., 2007). Similar records have been documented from Great Inagua where a distinctly erosional intra-MIS 5e has been documented (Thompson et al. (2011); Skrivanek et al. (2018). Blanchon et al. (2009). Blanchon et al. (2009) have noted in the Yucatan a similar intra MIS 5e discontinuity that they propose represents a drowning and backstep event as opposed to the base-level fall suggested for the Bahamian exposures. This complex record, which occurs within a 12,000–14,000 yr window between 130 and 134 and 118 ka, draws attention to a sub-Milankovitch glacioeustatic event that deviates from the general model of predictable precession-eccentricity forcing. Such changes may implicate nonperiodic, nonorbital mechanisms in sea-level and ice-volume changes in the interglacial records.

Important lessons from this complex Pleistocene interglacial stratigraphic record that relate to high-amplitude/high-frequency "icehouse" eustatic signals in the deep-time stratigraphic record include the following:

1. The "carbonate factory" is turned on as interglacial sea level floods the platform. Sediments are manufactured in shallow-marine environments and subsequently redistributed by tides, currents, waves, and wind. Subaerially, exposed carbonates indurate quickly and preserve evidence of sea-level and

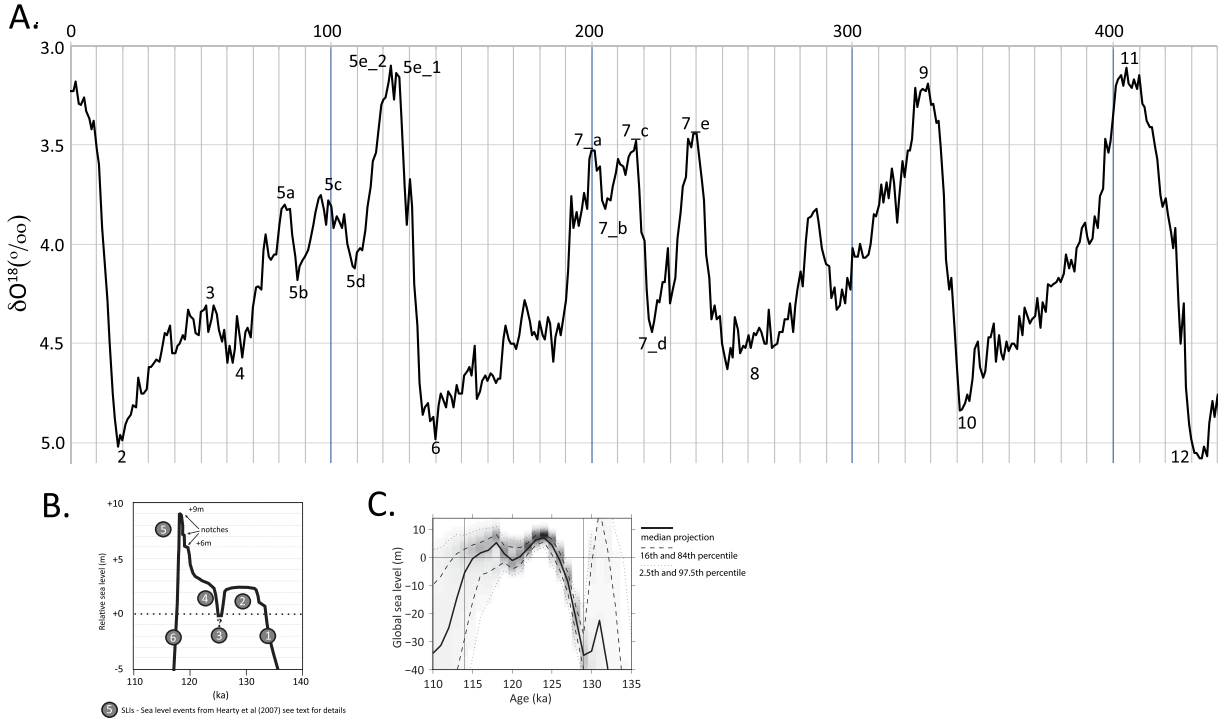

Fig. 3. Three different descriptors of Pleistocene sea level. (a) $\delta^{18}O$ curve from Lisiecki and Raymo (2005) showing position of main marine isotope stages; (b) detailed interpreted sea level of MIS 5e from Hearty et al. (2007) derived from observations from coastal sites worldwide as well as compilations from the literature; and (c) statistical compilation of sea-level positions by Kopp et al. (2009) illustrating in particular within shaded gray area the 80 percent confidence limit for sea-level position.

energetic changes. Karst, calcrete, and terra rossa soils form during prolonged exposure, particularly during lowstands.
2. As islands evolve, there is a dominance of lateral shingling (on- and offlapping) over vertical superposition (following work by Garrett and Gould, 1984).
3. The processes described in No. 2 above yield complex spatial–relative age relationships set up by nucleation of extensive younger "catenary" strandplains between anchoring headlands (e.g., Kindler and Hearty, 1997; their Fig. 2). Because lateral shingling is a key element, a simple model would suggest radial or concentric younging patterns away from an older core; in fact, in many cases, the older units occur on the periphery of the island complex—most likely the result of late interglacial sea-level rise shifting depocenters further inland relative to the seaward-younging strandplains. Additionally, major platform-margin collapse events can lead to complex margin morphologies (Mullins and Hine, 1989; Kindler and Hine, 2009).
4. Paleosol–caliche–calcrete surfaces typically bracket each major (short eccentricity) sequence. Paleosols darken in reddish hues (10 YR to 2.5 YR on the Munsell color chart) while increasing in clay content and degree of carbonate grain dissolution with age (Hearty, 1998), as driven by prolonged subaerial exposure and intercontinental aerosol Fe-clay and Si input during glacial maxima.
5. A combination of U–Th and AAR dates is essential for correlations between islands and for illustrating absolute and relative age relationships, respectively. These data are required because commonly relative character such as degree of weathering/cementation can vary spatially within a single island as a result of proximity to ocean spray (cf. Kindler, 1995), as well as changing rainfall and climate on a latitudinal scale.
6. Not all unconformity-bound successions can be linked to 20 or 100-ka-frequency insolation-driven glacioeustatic forcing, as distinct subdivisions within the MIS 5e point to more or less globally synchronous short-lived events (White et al., 1998; Hearty et al., 2007; Blanchon et al., 2009; Jackson et al., 2012). Such intra-interglacial variability demonstrates that cyclic depositional packages bounded by erosional unconformities such as the intra-MIS 5e record discussed here do not uniquely imply an insolation-driven glacioeustatic forcing. There is a significant chance that sub-Milankovitchian forcing plays a role in interglacial stratigraphic records.

3. Geologic setting of West Caicos

West Caicos is a 22.8 km^2 north–south-oriented, rhomboid-shaped island on the southwest corner of the Caicos Platform, Turks and Caicos, British West Indies. The Caicos Platform is situated on the southern end of the Bahamian archipelago between 21°57′ and 21°1′ North latitude, and between 71°29′ and 72°27' East longitude (Figs. 1 and 4), within the easterly trade winds and a very active hurricane track (Neuman et al., 1978; Wanless et al., 1988). The two dominant energy inputs that control deposition on the Caicos Platform are the northeast–southwest storm-generated open-ocean swells from the Atlantic, and the easterly trade winds along a deep margin that provide constant moderate wave action and agitation of bottom sediments across the entire Turks and Caicos platform (Lloyd et al., 1987; Wanless et al., 1988; Wanless and Dravis, 1989). The major reef tract and the high-relief islands of Providenciales, North Caicos, Middle Caicos, and East Caicos are set up facing the full energy of the northeast Atlantic swell (Wanless and Dravis, 1989; Rankey et al., 2009). In contrast, behind this northeast-facing energy barrier, the southern half of the platform—including the entire platform interior, Ambergris shoal, foreshore–shoreface systems like Long Bay Beach, and the strandplains on the east and north side of West Caicos—is more strongly influenced by the cross-platform easterly trade winds. This constant wind-driven wave energy is the source of roughly 90 percent of the sediment supply for the West Caicos dune–foreshore system from middle Pleistocene times to present day. It is important to note that the position of West Caicos on the leeward corner of the Caicos Platform, protected from the major Atlantic storm surge, results in a lower island relief; it was thus susceptible to near-total inundation during the upper MIS 5e transgression.

An additional control on modern depositional processes on West Caicos is the semi-arid setting, with rainfall of 50–60 cm/yr that is outpaced by evaporation that ranges from 150 to 170 cm/yr (Whitaker and Smart, 2004; Jones and Awiller, 2008). Interdune depressions on the east side of the island host Holocene evaporitic salinas with up to 10 cm of gypsum as well as very high magnesium calcite (proto-dolomite) (Morgan, 2008). Meteoric cementation and dissolution are also most significant, and in the older southern portion of the island, karst sinks are abundant.

Major physiographic features that will be referred to on West Caicos include, from northwest to southeast: Company Point Salina (recently excavated for a marina), northern Holocene strandplain, northeast dune ridge set, northwest hummocky terrain, west coast outcrop, west coast washover, central dune ridge or Railroad Ridge, southwest point, south coast outcrop, southern dune ridge complex, central lowlands, Lake Catherine, Great Salina, and east coast Holocene dune ridge/strandplain. Other key localities include Star Town, Boat Cove, and South Reef (Fig. 5).

The geology of West Caicos has been considered by Waltz (1988), Wanless and Dravis (1989), Dravis and Wanless (2008), and Simo et al. (2008). These studies presented initial maps and cross sections of the Holocene-Pleistocene stratigraphy of the island, identified a spectrum of Pleistocene reef, beach, and dune systems, and were able using morphostratigraphy (Wanless and Dravis (1989) and radiometric dating (Simo et al., 2008) to propose the presence of both MIS 5e and older Pleistocene units on the island. The combination of detailed surface cores (Waltz, 1988; Wanless and Dravis, 1989) and comparison to Holocene settings resulted in a model of island evolution that honors present-day observed processes including the setup of an initial central island spine that created a leeward protected setting for the MIS 5e reef system whose spectacular exposures dominate the west coast of the island. Later AAR and U–Th dating of material from some of the core material near boat cove led Kindler and Meyer (2012) to suggest that the older reef unit observed in the lower portion of one of the cores represents an older (MIS 11?) reef system. This unit is not shown on any of our maps as it does not outcrop anywhere on the island.

4. Mapping and analytical methods

4.1. Lidar and UAV models for base-map creation

Two different data sets have been used to create the base maps necessary for capturing the stratigraphic and facies patterns of West Caicos island. Georeferenced UAV-acquired photographs were used to create continuous-coverage SfM of the 9-km western and 2.4-km southern coastal outcrop at a resolution of ~5 pixels/cm depending on the area. UAVs were used to collect both plan-view and oblique images from elevations varying from 20 to 50 m (Fig. 6). The UAV photographs were georectified using differential GPS control points and merged together using Agisoft Photoscan Pro software to create a 3D point cloud. A triangular mesh was created from the point cloud, which enabled the construction of high-resolution photomosaics. The map-view photomosaics

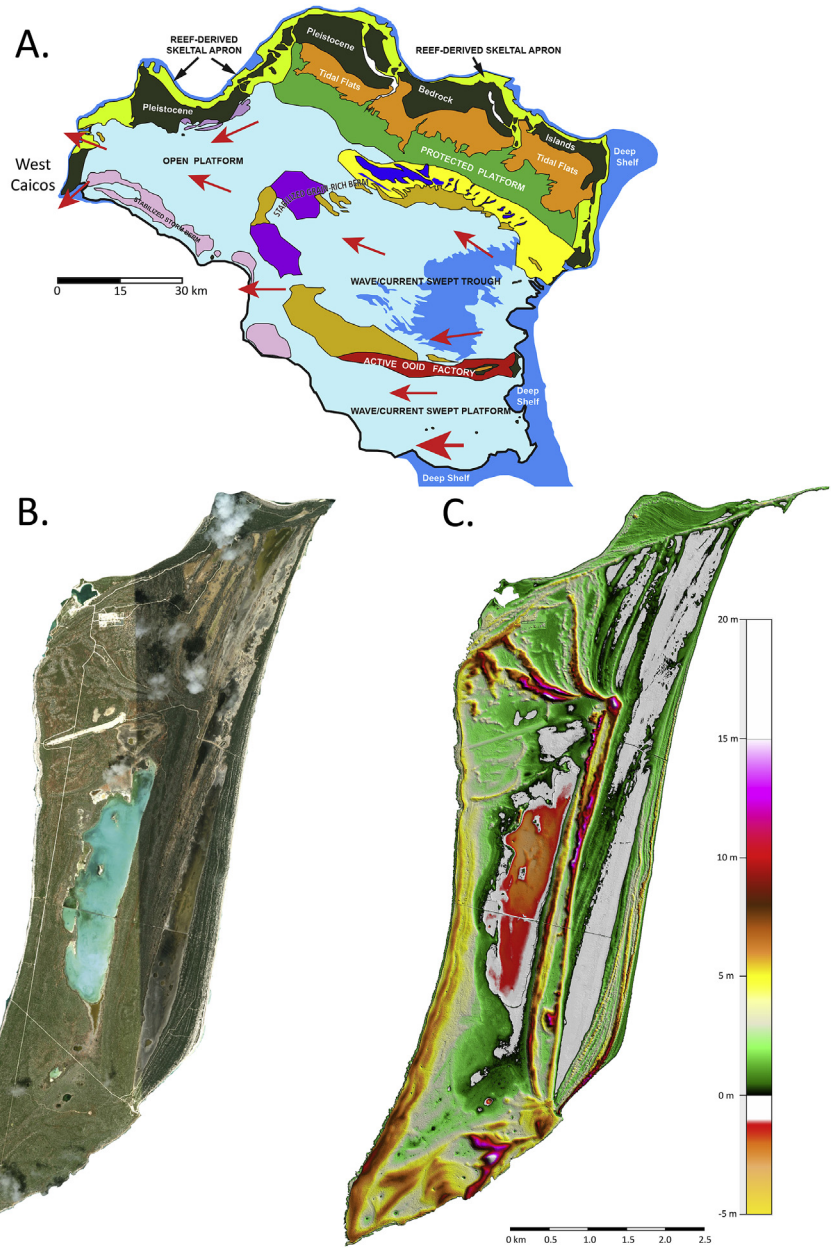

Fig. 4. (a) Generalized facies map for Caicos platform using data from Wanless and Dravis (1989) as well as satellite observations and detailed bottom sampling; (b) satellite image of West Caicos from Google Earth; and (c) DEM used to provide geomorphic base layer for unit mapping created from airborne lidar.

developed from this process served as a base for mapping at cm resolution. Field mapping was done by a group of three geologists using a standard facies key developed for this purpose.

The whole-island geologic map of West Caicos was accomplished by reconnaissance mapping of the island coupled with remote-sensing satellite imagery (2011 and 2014 Digital Globe images with 0.5- and 0.25-m resolution, respectively) and a recently collected airborne lidar data set. Comparison between the satellite image and the UAV-acquired photographs is significant (Fig. 6). However, the real breakthrough for creating the geologic map of the island came from the use of airborne lidar and the ability to create a bare-earth digital elevation model (BE-DEM). The resolution of the BE-DEM was not as high as the UAV-based SfM digital outcrop model, but the ability to remove the vegetation effect made this approach superior to both the UAV and satellite images (compare Fig. 4B and C). Using the combination of ground-truth information from the coastal exposures and limited road cuts on the island, the UAV-acquired SfM models and photographs, available satellite imagery, and lidar, we were able to establish the stratigraphy using concepts of morphostratigraphy, superposition, relationship of headland anchors and catenary beaches (limited), caliche profiles, and relative and radiometric age determinations. Sea level above [+] and below [-] present, based on facies transitions, are referenced to the modern sea-level datum with an estimated error of ±0.2 m.

A useful aspect of the DEM created from the lidar "point cloud" [lingo?] is the ability to generate topographic profiles that can then be used as a guide to construct geologic cross sections, especially in these young systems where the geomorphic surface relates closely to the stratigraphic elements. The combination of a detailed geologic map using UAV photography and then the generation of 200-m laterally spaced topographic profiles along the entire 8.4 km

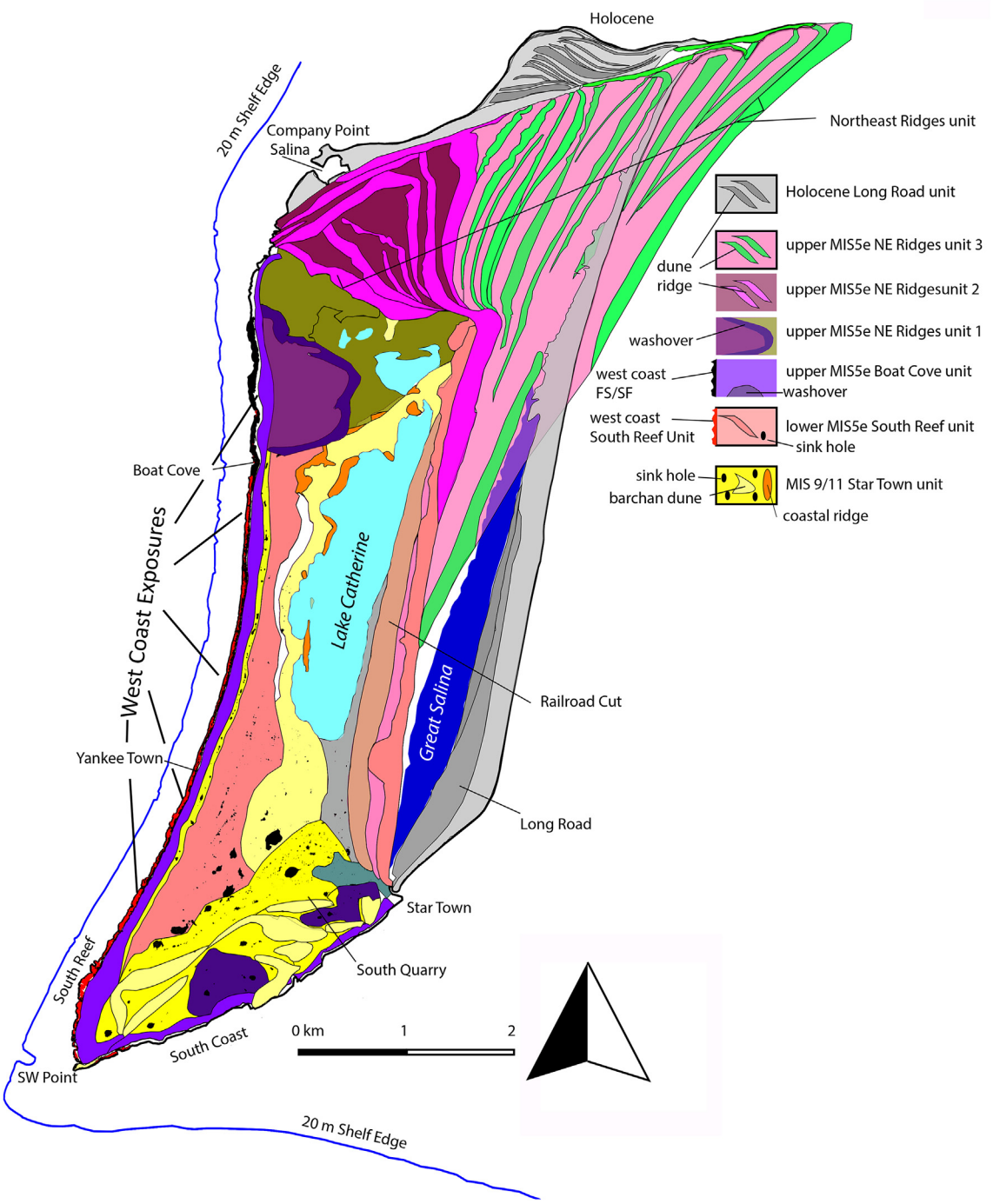

Fig. 5. Geologic map of West Caicos and proximal offshore combining ground observations and lidar-based geomorphology and showing the spatial arrangement of stratigraphic units as well as named localities. Offshore imaging is seen using green-laser-based bathymetric data.

of the west coast outcrop allowed creation of a spatially correct cross section used later in our discussion of the MIS 5e west coast stratigraphy.

4.2. AAR: whole-rock aminostratigraphy

Amino acid racemization (AAR) geochronology is an effective biogeochemical tool for stratigraphic correlations and can yield numerical age estimates where the rate of racemization is independently calibrated (Murray-Wallace, 2018). The AAR method is based on the racemization of amino acids preserved in biominerals. Through time, L-isomer amino acids racemize to their D-isomer form. The ratio of D/L measures the extent of racemization and increases to an equilibrium ratio with time and other variables after death of the organism. In living organisms, the D/L ratio is initially zero (±0.01 with laboratory preparation) and increases to an equilibrium ratio of 1.00.

Like other chemical reactions, the rate of racemization depends on time and the ambient temperature of the reaction medium. Thus, diligent and consistent collection methods are critical to determination of reliable data sets (Hearty and Kaufman, 2000, 2009). In addition to independent molecular factors, the rate of the

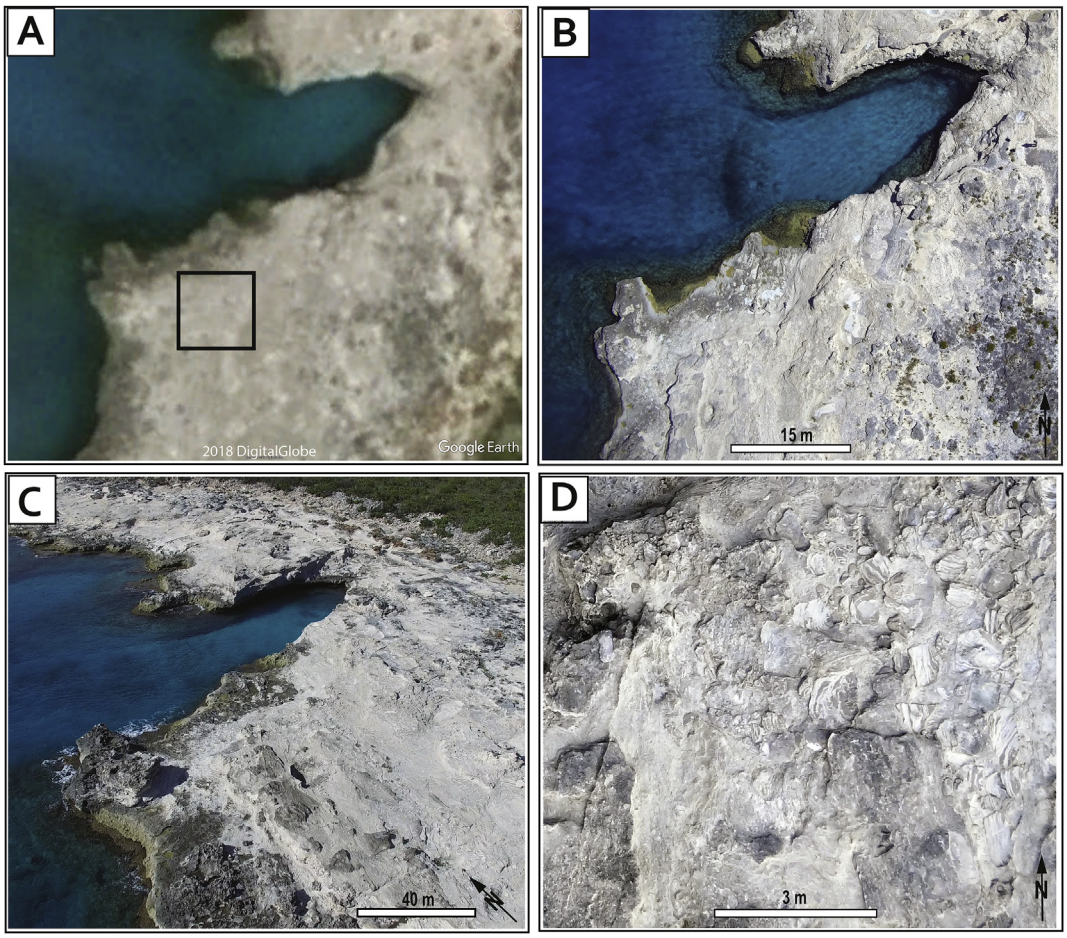

Fig. 6. Comparison of satellite and UAV imagery to highlight difference in resolution. (a) Satellite imagery; (b) UAV imagery at same scale; (c) UAV imagery at 30-m elevation; and (d) zoomed image of UAV image showing centimeter to decimeter resolution of beachrock conglomerate facies.

racemization reaction depends on the ambient temperature within the geologic deposit. At microscale, more deeply buried samples are more representative of the integrated temperature history at the site. Surface and shallowly buried samples experience greater net heating and would be expected to yield spuriously higher D/L values. For these reasons, on a macro-regional scale, the racemization rate at more southerly sites (as in the Bahamas) is expected to be somewhat greater than that at cooler and more northerly islands (Hearty and Kaufman, 2000; their Fig. 3).

Recent advances in whole-rock sample analysis, employing the traditional ion exchange (IE) high-performance liquid chromatography methods (HPLC), opened new areas of research on dune and marine sediments (e.g., Hearty and Kaufman, 2000). More recently, the reverse-phase chromatography (RPC) HPLC technique (Kaufman and Manley, 1998; Kaufman, 2003) made it possible to analyze microscopic samples (<0.1 mg) such as single ostracods (Kaufman, 2003), foraminifera (Hearty et al., 2004; Kaufman, 2006), or individual ooids (Hearty et al., 2006). Traditional IE methods, primarily focused on the epimerization of alloisoleucine/isoleucine (A/I), were far more labor intensive and have been largely supplanted by the highly automated RPC technology, which we employ in this study.

The RPC technique determines the extent of racemization (here using primarily D/L aspartic (Asp) and glutamic (Glu) acids, but also D/Ls of isoleucine and valine) from orders-of-magnitude smaller samples compared to those of the IE. For comparison with previous studies employing traditional IE methods yielding A/I values (e.g., Hearty and Dai Pra, 1992), we have converted several of our D/L Glu values from major units to A/I using the equations established in Whitacre et al. (2017; their Fig. 1 showing IE vs RPC) for comparison between techniques.

Whole-rock sample preparation procedures are detailed in Hearty and Kaufman (2000). Samples were gently disaggregated and repeatedly sieved to obtain the 250- to 850-μm fraction. This size range excludes fine intergranular cements that have been abraded from grains, as well as large or degraded grains that could significantly influence the A/I ratio. Microscopic examination confirms the separation of grains from cements. Sample analyses performed at Northern Arizona University followed standard procedures described in Kaufman and Manley (1998) and Kaufman (2003). A database of several hundred whole-rock analyses and age models derived from samples from Bahamas and Bermuda is available in several publications (Hearty and Kaufman, 2000; Hearty et al., 2007). Because the whole-rock method analyzes mixed aggregates of skeletal or coated grains that form over time (i.e., having an “inherited age”), entirely “modern” material is not expected. Results of analyses on West Caicos are given in Table 1.

4.3. U–Th coral geochronology

Material for U–Th dating was collected by initially examining material in the field for the most pristine samples with no visible later blocky calcite spar. Secondarily, following slabbing of coral material, surface trace-element scans were undertaken at the

Table 1
Reverse phase chromatography (RPC) analytical results of D/L values from whole rock (WR) samples from West Caicos and Providenciales. Samples are grouped by stratigraphic units from which they were collected. Conversions from D/L to A/I were made according to formulae in Whitacre et al. (2017). We conclude that conversion of D/L Glu yields the most representative A/I values, based on previous studies in the southern Bahamas. WR samples were prepared at U. Texas and analyzed according to standard procedures at the Amino Acid Geochronology Laboratory, Northern Arizona University (D. Kaufman, Director).

UAL	Field ID	Fraction	Location	D/L Glu	Est A/I from D/L Glu	D/L Asp	A/I from D/L Asp	D/L Ala	A/I from D/L Ala	D/L Val	A/I from D/L Val	D/L Ile	A/I from D/L Ile
Holocene (MIS 1)													
15051	CS-HB-01	250	East active beach	0.183	0.238	0.043	0.087	0.213	0.059	0.052	0.037	0.055	0.039
15045	Cs rz-0	125	N coast mod	0.187	0.267	0.059	0.091	0.223	0.064	0.063	0.046	0.063	0.047
15098	CSHB2	250	East active beach	0.198	0.230	0.040	0.101	0.216	0.060	0.054	0.039	0.061	0.045
15722B	CSRTZ-1AN	250	AN	0.203	0.300	0.080	0.106	0.283	0.094	0.072	0.055	0.073	0.055
15046	Cs rz-0b	125	N coast mod	0.209	0.295	0.076	0.112	0.245	0.074	0.068	0.051	0.069	0.052
15726B	CSCC-1AN	250	East recent	0.209	0.266	0.058	0.112	0.274	0.089	0.060	0.044	0.063	0.047
15067	CSCP3	250	Camp N	0.216	0.305	0.083	0.119	0.299	0.103	0.090	0.070	0.103	0.084
15074	Cslr-5	125	Long Road	0.219	0.289	0.072	0.121	0.319	0.114	0.081	0.062	0.073	0.056
15092	CSST2	125	Star Town HB	0.221	0.278	0.065	0.123	0.307	0.108	0.083	0.064	0.083	0.065
15047	Cs rz-1	125	N coast mod	0.222	0.320	0.094	0.125	0.328	0.119	0.098	0.078	0.087	0.069
15071	Cslr-2	125	Long Road	0.225	0.309	0.086	0.128	0.314	0.112	0.092	0.072	0.093	0.074
15065	CSCP1	125	Camp N	0.226	0.333	0.105	0.129	0.310	0.109	0.090	0.070	0.090	0.071
15070	Cslr-1	125	Long Road	0.226	0.274	0.063	0.129	0.309	0.109	0.092	0.072	0.094	0.075
15066	CSCP2	250	Camp N	0.227	0.319	0.094	0.130	0.329	0.120	0.099	0.079	0.096	0.077
15073	Cslr-4	125	Long Road	0.229	0.303	0.082	0.132	0.329	0.120	0.097	0.077	0.097	0.078
15068	CSCP4B	125	Camp N	0.230	0.335	0.107	0.133	0.347	0.132	0.104	0.083	0.108	0.089
15048	Cs rz-2	125	N coast mod	0.232	0.329	0.102	0.135	0.326	0.119	0.099	0.078	0.101	0.081
15072	Cslr-3	125	Long Road	0.238	0.318	0.093	0.142	0.348	0.132	0.106	0.085	0.117	0.098
15052	CS-NE 14	250	N coa	0.251	0.366	0.135	0.157	0.322	0.116	0.133	0.110	0.145	0.126
N=19			**Means**	**0.219**	**0.122**								
				±0.017	**±0.017**								
MIS 5e Skeletal Reef matrix of South Reef unit													
15723B	CSSR-1AN	125	South Reef	0.397	0.512	0.325	0.366	0.644	0.362	0.257	0.235	0.220	0.207
15724B	CSSR-2AN	125	South Reef	0.399	0.503	0.311	0.369	0.649	0.366	0.289	0.269	0.283	0.278
15725B	CSSR-3AN	250	South Reef	0.421	0.524	0.346	0.409	0.711	0.425	0.299	0.280	0.288	0.285
15089	CSSR3	250	South Reef	0.424	0.454	0.237	0.413	0.693	0.408	0.307	0.288	0.332	0.336
N=5			**Means**	**0.404**	**0.506**								
				±0.019	**±0.032**								
MIS 5e Complex (South Reef, Boat Cove, and NE Ridge Set units)													
15716B	CSTC 1	250	Provo Rd west	0.387	0.483	0.279	0.349	0.704	0.419	0.292	0.271	0.294	0.291
15055	Csaq-1b	125	Airport Q	0.428	0.565	0.421	0.421	0.601	0.323	0.271	0.250	0.291	0.288
15057	Csaq-1e	250	Airport Q	0.409	0.465	0.252	0.386	0.582	0.306	0.248	0.225	0.273	0.267
15091	CSST1	250	Star Town LIG	0.419	0.463	0.250	0.405	0.673	0.389	0.284	0.263	0.296	0.294
15090	CSSR4	250	South Reef	0.430	0.466	0.254	0.425	0.690	0.405	0.297	0.277	0.310	0.310
15081	CSNE3	250	Northeast	0.432	0.478	0.271	0.428	0.685	0.401	0.321	0.302	0.371	0.385
15079	CSNE17A	250	Northeast	0.434	0.495	0.298	0.432	0.670	0.386	0.308	0.289	0.345	0.352
15710B	CSFL 1	250	Flamingo Lake	0.440	0.508	0.319	0.442	0.796	0.512	0.365	0.351	0.350	0.359
15084	Csor-2	125	Ridge at knot	0.442	0.477	0.270	0.446	0.690	0.405	0.319	0.301	0.365	0.377
15727B	CSRR-3	250	Rail road grade	0.443	0.501	0.307	0.449	0.790	0.506	0.375	0.362	0.342	0.348
15061	CSBC1A	250	Boat cove	0.447	0.477	0.269	0.456	0.721	0.435	0.322	0.304	0.361	0.372
15041	Cs pq-1d	250	Power Q	0.449	0.465	0.253	0.460	0.736	0.450	0.333	0.316	0.374	0.388
15095	CSSW1C	425	Southwest point	0.450	0.483	0.278	0.462	0.714	0.429	0.312	0.293	0.351	0.359
15064	CSBC5B	250	Boat Cove	0.450	0.485	0.282	0.462	0.730	0.444	0.327	0.309	0.368	0.380
15042	Cs pq-1e	250	Power Q	0.450	0.489	0.288	0.462	0.730	0.444	0.331	0.314	0.373	0.387
15053	CSAN1	250	Cut So of PS	0.451	0.500	0.306	0.463	0.710	0.424	0.329	0.311	0.363	0.375
15086	Csps-2	250	South Power	0.452	0.481	0.277	0.465	0.749	0.463	0.337	0.320	0.369	0.382
15729B	CSRR-5	250	Railroad LIG	0.452	0.518	0.335	0.465	0.692	0.407	0.303	0.283	0.284	0.280
15080	CSNE2	250	Northeast	0.454	0.468	0.257	0.469	0.737	0.451	0.345	0.329	0.372	0.385
15087	CSSR2-(BUSF)	250	South Reef	0.454	0.511	0.324	0.470	0.725	0.439	0.348	0.332	0.387	0.404
15060	Csas-1c	250	Cut E- Boat Cove	0.455	0.500	0.305	0.471	0.726	0.440	0.331	0.313	0.369	0.382
15075	CSNE1	250	Northeast	0.455	0.496	0.299	0.471	0.721	0.436	0.340	0.323	0.369	0.382
15139	CSPS4	250	South Power	0.455	0.471	0.261	0.472	0.743	0.458	0.338	0.321	0.381	0.396
15076	CSNE16A	250	NE peninsula	0.456	0.502	0.309	0.473	0.717	0.431	0.349	0.334	0.394	0.413
15085	Csps-1	250	Power Sta South	0.456	0.502	0.309	0.474	0.741	0.455	0.348	0.332	0.404	0.426
15039	Cs pq-1b	250	Power Quarry	0.456	0.476	0.269	0.474	0.754	0.468	0.343	0.327	0.386	0.403
15040	Cs pq-1c	250	Power Quarry	0.457	0.478	0.271	0.475	0.737	0.451	0.332	0.315	0.380	0.396
15038	Cs pq-1a	250	Power Quarry	0.457	0.471	0.261	0.475	0.766	0.481	0.341	0.325	0.387	0.404
15088	CSSR2A	250	South Reef	0.460	0.489	0.289	0.480	0.704	0.418	0.325	0.307	0.364	0.375
15097	CSSW2C	250	SW cape	0.461	0.486	0.284	0.483	0.698	0.413	0.312	0.293	0.344	0.351
15050	CS sr 1B	250	South Reef	0.463	0.483	0.278	0.486	0.696	0.411	0.319	0.301	0.352	0.361
15094	CSSW1B	250	SW cape	0.464	0.497	0.301	0.488	0.719	0.433	0.331	0.314	0.360	0.371
15062	CSBC1B	250	Boat Cove	0.464	0.495	0.297	0.488	0.743	0.457	0.343	0.327	0.376	0.391
15083	Csor-1	250	Ridge at knot	0.465	0.470	0.259	0.492	0.745	0.459	0.355	0.341	0.393	0.412
15728B	CSRR-4	250	Railroad?	0.466	0.528	0.352	0.492	0.797	0.513	0.349	0.333	0.339	0.345
15078	CSNE17B	250	NE peninsula	0.467	0.513	0.326	0.495	0.770	0.485	0.354	0.339	0.397	0.417
15058	Csas-1a	250	E of Boat Cove	0.467	0.530	0.356	0.495	0.748	0.462	0.359	0.344	0.395	0.414
15077	CSNE17C	250	NE peninsula	0.467	0.506	0.316	0.495	0.763	0.478	0.360	0.346	0.409	0.431
15059	Csas-1b	250	cut E of Boat Cove	0.470	0.503	0.311	0.500	0.732	0.446	0.344	0.328	0.380	0.396
15043	Cs RR-1	250	Railroad	0.471	0.492	0.293	0.502	0.770	0.485	0.370	0.357	0.422	0.448
15082	CSNE4	250	Northeast	0.471	0.492	0.292	0.503	0.788	0.504	0.378	0.366	0.411	0.434
15709B	CSBC 1C	250	Boat Cove	0.474	0.524	0.346	0.509	0.783	0.498	0.351	0.335	0.314	0.315
15056	Csaq-1d	250	Airport Q top	0.480	0.521	0.341	0.520	0.740	0.454	0.336	0.319	0.369	0.381
N=46			**Means**	**0.453**	**0.468**								
				±0.015	**±0.027**								
Railroad Ridge (Early MIS 5e)													
15721B	CSRW-2	250	Runway	0.489	0.539	0.372	0.538	0.763	0.478	0.338	0.321	0.311	0.312
15730B	CSRR-6	250	Railroad Ridge	0.518	0.552	0.397	0.599	0.797	0.514	0.405	0.395	0.422	0.448
15044	Cs rr-2	125	Railroad Ridge	0.534	0.545	0.383	0.634	0.768	0.483	0.405	0.396	0.461	0.498
15049	Cs sq-2	250	South Quarry	0.541	0.579	0.449	0.648	0.751	0.465	0.424	0.417	0.464	0.501
N=4			**Means**	**0.521**	**0.605**								
				±0.023	**±0.049**								
Star Town Unit (MIS 9/11)													
15069	CSDL2	250	Do not know loc?	0.576	0.577	0.446	0.730	0.849	0.569	0.515	0.522	0.582	0.656
15054	Csaq-1a	250	Airport Quarry	0.580	0.599	0.492	0.739	0.881	0.604	0.474	0.474	0.543	0.604
15720B	CSRW-1	250	Runway Q	0.592	0.660	0.634	0.766	0.944	0.677	0.500	0.504	0.501	0.549
15719B	CSTL 3	250	Provo Taylor Rd	0.599	0.619	0.535	0.783	0.932	0.663	0.575	0.591	0.587	0.664
15715B	CSNP 2	250	Provo Chalk Sd	0.603	0.633	0.568	0.794	0.935	0.667	0.559	0.573	0.582	0.656
15718B	CSTL 1	250	Provo Taylor Rd	0.614	0.622	0.543	0.821	0.969	0.707	0.593	0.614	0.578	0.652
15096	CSSW2	250	SW point	0.635	0.600	0.494	0.875	0.954	0.689	0.573	0.590	0.668	0.774
15714B	CSNP 1	250	Provo Chalk Sd	0.639	0.651	0.613	0.885	0.966	0.703	0.568	0.584	0.541	0.601
15093	CSST3	125	Star Town mP	0.655	0.675	0.674	0.926	0.909	0.636	0.587	0.606	0.622	0.711
N=9			**Means**	**0.610**	**0.814**								
				±0.028	**±0.069**								

Bruker Technology facility in Madison, Wis., for Sr trace-element concentration. Modern aragonitic corals have high (6000–10,000 ppm) Sr concentrations, whereas those altered to low-Mg calcite through diagenesis more typically have a few-hundred-ppm Sr. Thus, if trace-element maps showed Sr concentrations in the 6000–10,000 ppm range, we assumed little or no alteration of the material. This technique is particularly useful as it maps the entire surface of the coral and then allows a more well-constrained selection of sample sites for U–Th analysis. The careful analysis of areas of greater alteration was required as XRD analysis of these coral samples showed a range of calcitization from 100% calcite to 3% calcite, indicating that in patches, extensive diagenesis has occurred and will have impacted the results of the dating.

All analyses were run in the Institute of Global Environmental Change, Xi'an Jiaotong University, Xi'an, China, by the group of Hai Cheng (Table 2) (Edwards et al., 1987; Cheng et al., 2013). For each of the 19 coral samples reported here, approximately 30 mg of power drilled from the fossil coral was weighed and then dissolved slowly by drop-wise addition of nitric acid. After dissolution, all samples were spiked with a mixed ^{233}U–^{236}U–^{229}Th spike; then, two drops of $HClO_4$ were added to the solution, which was then dried down, taken up in 2N HCl, and transferred to 15-ml centrifuge tubes along with a 2N HCl rinse. One drop of dissolved Fe and six to nine drops of NH_4OH were added to raise pH to 8–8.5, at which time iron (oxy) hydroxide precipitated. This precipitate was then centrifuged, decanted, washed with deionized H_2O (>18MΩ), centrifuged again, dissolved in 14M HNO_3, and transferred to a Teflon beaker. It was then dried down and taken up in 7N HNO_3 for anion-exchange chromatography using AG1-X8, 100–200 mesh resin, and a polyethylene frit. Initial separation was done on Teflon columns with a 0.55-ml column volume (CV). The sample was loaded in one CV of 7N HNO_3, followed by 1.5 CV of 7N HNO_3, 4 CV of 6N HCl (collect Th fraction), and 4 CV of deionized H_2O (collect U fraction). The Th and U fractions were then dried down in the presence of two drops of $HClO_4$ and dissolved in weak nitric acid for analysis on the mass spectrometer.

Concentrations of U and Th isotopes were calculated by isotope dilution using nuclide ratios determined on a Thermo Finnigan Neptune mass spectrometer. All measurements were done, using a peak jumping routine in ion-counting mode, on the discreet dynode multiplier behind the retarding potential quadrupole. Each sample measurement was bracketed by measurement of an aliquot of a wash solution, used to correct instrument background count rates on the masses measured. The long-term repeatability for ($^{234}U/^{238}U$) of CRM112a is 1.2‰ (2 S.D. n = 129). This measured $\delta^{234}U$ is −38.3 (±1.2), which is in agreement with the certificate value −38.5 (±1.5). Half-lives used in this study are 245.620 ka and 75.584 ka (Cheng et al., 2013).

5. Stratigraphic framework of West Caicos

The stratigraphic framework for the island highlights six units (Figs. 2, 5 and 8). These units will be described individually from oldest to youngest, starting with the MIS 9/11 Star Town unit, followed by the four MIS 5e subunits (Railroad Ridge, South Reef, Boat Cove, and Northeast Ridges set) and, finally, the Holocene Long Road unit.

Table 2
U/Th Dating Results for Coral Samples from the west coast of West Caicos (located).

samples with initial δ234U above 160‰, which are not used

^{230}Th dating results. The error is 2σ error.

Sample Number	^{238}U (ppb)	^{232}Th (ppt)	$^{230}Th/^{232}Th$ (atomic x10^{-6})	$\delta^{234}U$* (measured)	$^{230}Th/^{238}U$ (activity)	^{230}Th Age (yr) (uncorrected)	^{230}Th Age (yr) (corrected)	$\delta^{234}U_{initial}$** (corrected)	^{230}Th Age (yr BP)*** (corrected)
South Reef Area - South Reef Unit (Lower MIS 5e)									
CS-SW-1D	1455.3 ±1.7	48 ±6	396195 ±46391	141.4 ±1.7	0.7896 ±0.0022	123740 ±727	**123739 ±727**	200 ±2	123672 ±727
CS-SW-1A-A-Palmata (A)	2369.4 ±2.9	954 ±20	31549 ±662	106.1 ±1.6	0.7705 ±0.0019	126297 ±681	**126287 ±680**	152 ±2	126220 ±680
CS-SR-1A	2927.5 ±5.0	29 ±16	1323080 ±707584	118.7 ±2.0	0.7949 ±0.0021	130650 ±825	**130649 ±825**	172 ±3	130582 ±825
CS-SR-1B (A)	2127.1 ±2.3	537 ±11	49859 ±1054	108.3 ±1.6	0.7630 ±0.0015	123559 ±573	**123553 ±572**	154 ±2	123486 ±572
CS-SR-1D (MA)	1722.3 ±1.4	123 ±6	176048 ±7941	106.7 ±1.3	0.7656 ±0.0010	124687 ±417	**124685 ±417**	152 ±2	124618 ±417
AB Transect (Lower (AB-10-E) and Upper MIS 5e (AB-4, 5B, 6, 10)									
Boat Cove Unit (Upper MIS 5e)									
CS-AB-4 (M)	1304.7 ±1.2	602 ±13	25517 ±534	108.5 ±1.3	0.7141 ±0.0009	110006 ±345	**109994 ±345**	148 ±2	109926 ±345
CS-AB-5B (M)	909.2 ±0.7	103 ±4	108924 ±4429	107.6 ±1.4	0.7478 ±0.0015	119314 ±530	**119311 ±530**	151 ±2	119245 ±530
CS-AB-6 (M)	817.4 ±1.2	70 ±7	147084 ±14350	106.6 ±2.8	0.7610 ±0.0031	123367 ±1109	**123365 ±1109**	151 ±4	123299 ±1109
CS-AB-10 (M)	2633.4 ±3.3	108 ±5	304837 ±14305	105.5 ±1.7	0.7555 ±0.0017	122016 ±634	**122015 ±634**	149 ±2	121949 ±634
South Reef Unit (Lower MIS 5e)									
CS-AB-10-E (A)	1094.7 ±1.3	61 ±6	233202 ±23172	103.8 ±2.3	0.7856 ±0.0027	131547 ±1034	**131545 ±1034**	150 ±3	131479 ±1034
CS-AB-22	2256.2 ±1.9	184 ±5	162711 ±4602	119.8 ±1.3	0.8045 ±0.0015	133374 ±578	**133372 ±578**	174 ±2	133306 ±578
Boat Cove Area - Boat Cove Unit (Upper MIS 5e)									
Diploria	1421.9 ±1.9	565 ±13	30483 ±696	105.9 ±1.9	0.7345 ±0.0025	115979 ±800	**115968 ±800**	147 ±3	115902 ±800
CS-BC-1 (D)	2239.9 ±2.0	367 ±10	76113 ±2121	106.2 ±1.3	0.7562 ±0.0010	122038 ±424	**122034 ±424**	150 ±2	121968 ±424
CS-BC-2 (D)	1824.5 ±1.6	258 ±12	87977 ±4161	105.9 ±1.3	0.7547 ±0.0012	121682 ±453	**121678 ±453**	149 ±2	121612 ±453
CS-BC-3 (D)	1197.8 ±0.9	3170 ±64	4819 ±98	116.3 ±1.3	0.7737 ±0.0013	124833 ±486	**124767 ±488**	165 ±2	124701 ±488
CS-BC-3 (M)	662.1 ±0.9	293 ±7	29123 ±679	110.1 ±2.1	0.7808 ±0.0027	128468 ±974	**128457 ±974**	158 ±3	128391 ±974
CS-BC-4 (D)	1056.3 ±0.9	2232 ±46	5913 ±122	106.6 ±1.4	0.7579 ±0.0015	122458 ±538	**122404 ±539**	151 ±2	122338 ±539
MIS 9/11 Star Town Unit									
CS-SQ-1	2215.8 ±2.2	980 ±20	39008 ±797	61.3 ±1.2	1.0461 ±0.0013	368962 ±5571	**368949 ±5571**	174 ±4	368881 ±5571
CS-SQ-1B	432.9 ±0.3	73 ±4	101867 ±5826	61.9 ±1.1	1.0456 ±0.0013	365376 ±5321	**365370 ±5320**	174 ±4	365302 ±5320

U decay constants: $\lambda_{238} = 1.55125 \times 10^{-10}$ (Jaffey et al., 1971) and $\lambda_{234} = 2.82206 \times 10^{-6}$ (Cheng et al., 2013). Th decay constant: $\lambda_{230} = 9.1705 \times 10^{-6}$ (Cheng et al., 2013).

*$\delta^{234}U = ([^{234}U/^{238}U]_{activity} - 1) \times 1000$. ** $\delta^{234}U_{initial}$ was calculated based on ^{230}Th age (T), i.e., $\delta^{234}U_{initial} = \delta^{234}U_{measured} \times e^{\lambda_{234} \cdot T}$

Corrected ^{230}Th ages assume the initial $^{230}Th/^{232}Th$ atomic ratio of 4.4 ±2.2 x10^{-6}. Those are the values for a material at secular equilibrium, with the bulk earth $^{232}Th/^{238}U$ value of 3.8. The errors are arbitrarily assumed to be 50%.

***B.P. stands for "Before Present" where the "Present" is defined as the year 1950 A.D.

(A) *Acropora palmata*, (D) *Diploria strigosa*, (M) *Montastrea, (Ma) Madresas*

5.1. Star Town unit: middle Pleistocene

The southern coast and southern 25 percent of the island of West Caicos is dominated by a newly recognized Pleistocene unit called here the *Star Town unit* after a small relict settlement and quarry cut on the southeast corner of the island (Fig. 5). The Star Town exposures that form the rugged 4–5-m-high bluffs on the south coast of West Caicos are composed of well-lithified grainstones, including skeletal, peloidal, and some oolitic facies. The vertical succession of sedimentary facies/structures in these

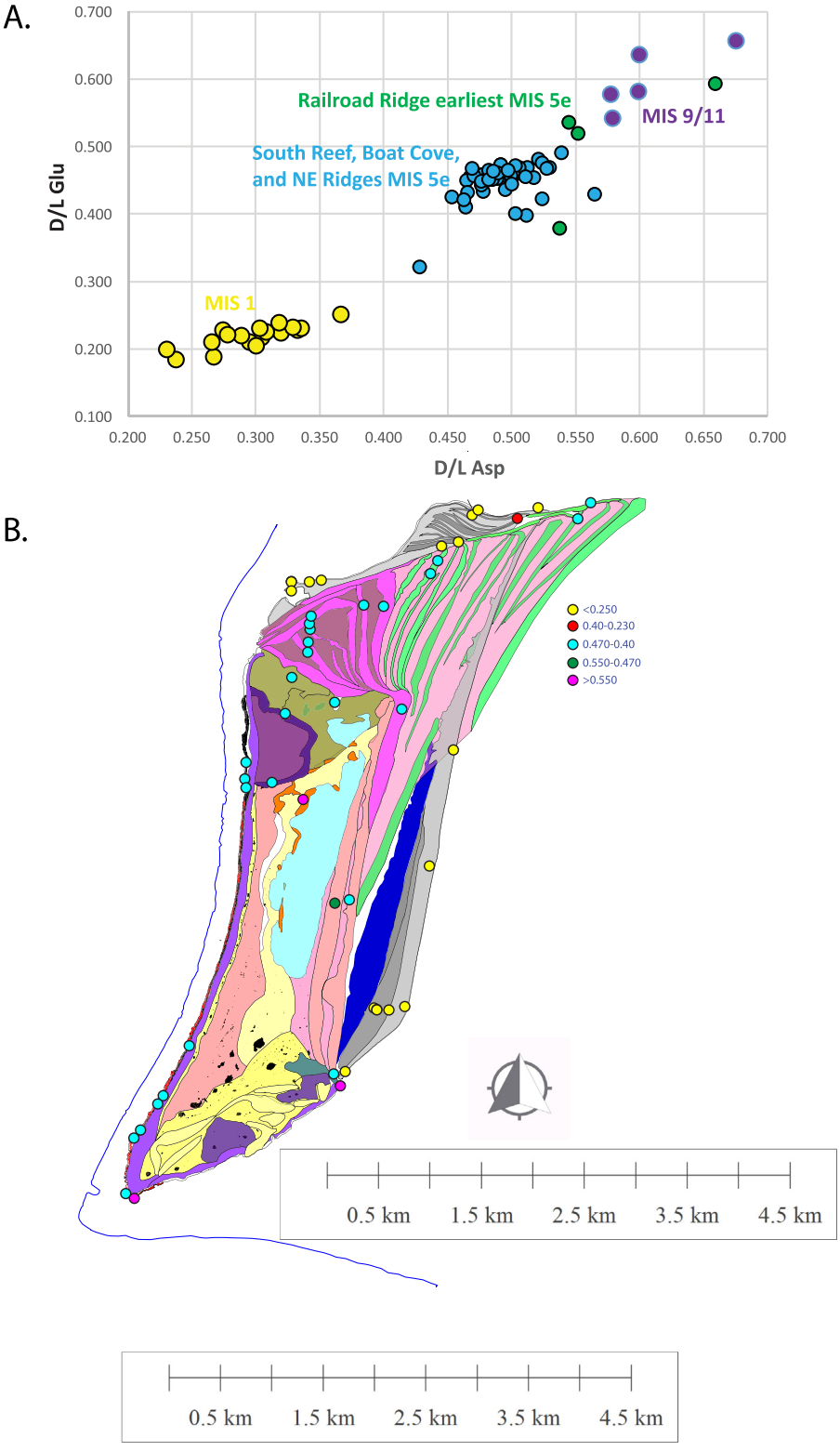

Fig. 7. D/L Glu vs D/L Asp ratio data from West Caicos showing link between units and relative ages. (a) Cross-plot of D/L Glu vs D/L Asp showing covariance of data; and (b) map distribution of D/L ratio data showing correspondence between five major groupings of D/L AAR data: <0.250–Holocene, 0.45–0.250 early Holocene, 0.47–0.45 MIS 5e, 0.550–0.470 early MIS 5e or possibly 7, and >0.550 MIS 9/11.

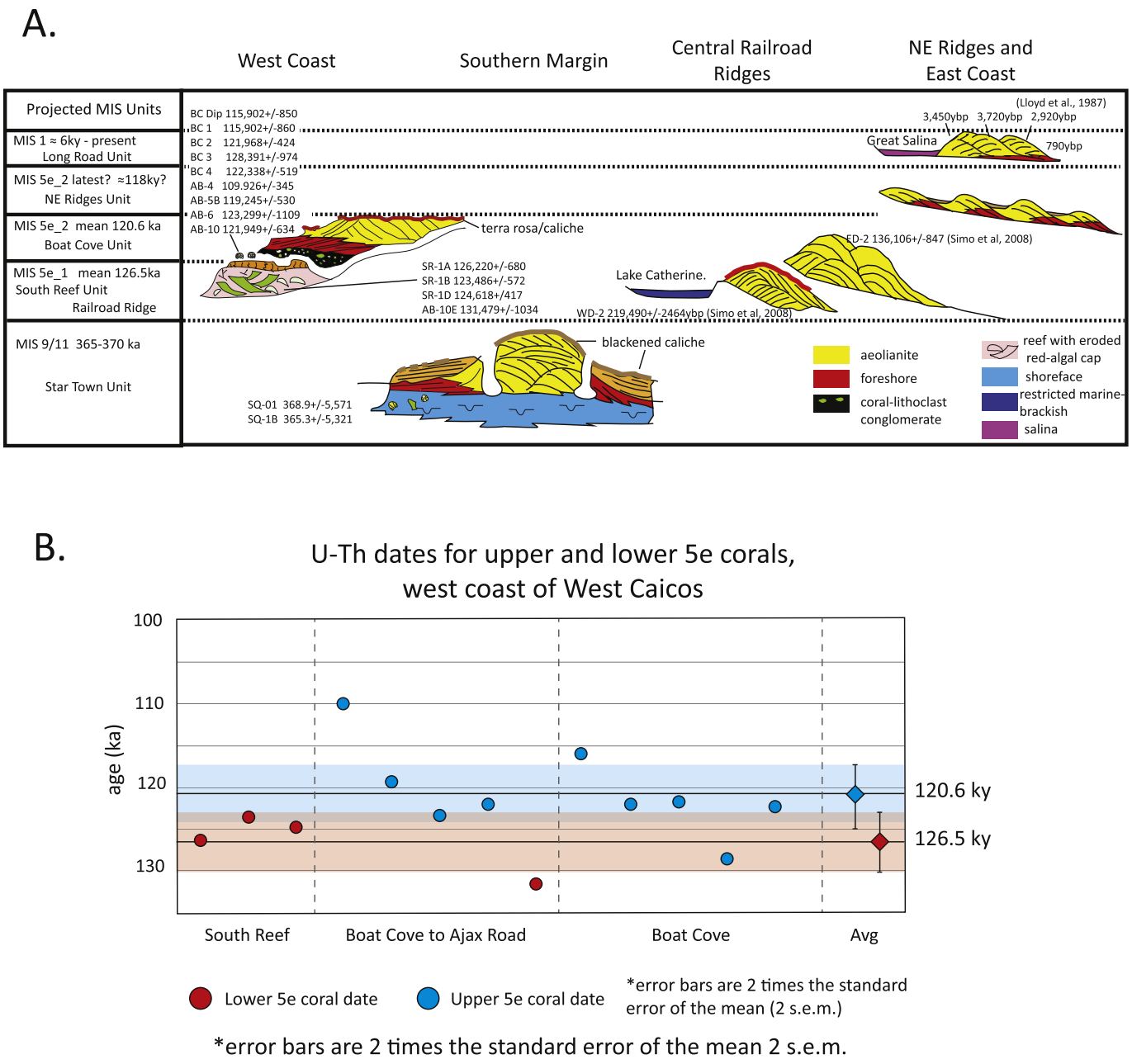

Fig. 8. (a) Relative age in space (pseudo–Wheeler diagram) of the six units discussed in text: Star Town, Railroad Ridges, South Reef, Boat Cove, Northeast Ridges, and Long Road. Age constraints come from both previously published literature and results from this study. Note that nearly all U–Th ages are summarized. (b) Detail of lower vs. upper MIS 5e coral ages emphasizing statistically significant separation of lower vs. upper MIS 5e.

exposures begins with massive to burrowed fabrics in the first 1–2 m above sea level, succeeded upward by south-dipping, foreshore, swash-stratified facies at approximately 2–3 m above sea level, and then capped locally by high-angle eolian cross-stratification with extensive rhizoconcretions (Fig. 9).

At the southwest tip of West Caicos (SW Point, Fig. 5) Star Town strata that were traced continuously across the southern bluff exposures of the island are unconformably overlain by encrusting coral, coastal megabreccias, foreshore facies, and thin eolianites of the younger South Reef unit (Figs. 8A, 10 and 11). The sharp, wave-polished surface of the Star Town grainstone in this area testifies to pre–South Reef marine erosion that removed the top–Star Town calcrete present to the east (Fig. 11A). The low-angle, seaward-dipping foreshore grainstones of the Star Town dip to the south (present-day seaward) on the south coast of the island and wrap around the southwest tip of the island, where they dip to the northwest–north, indicating that the present-day island coast mimics this middle Pleistocene geometry (Fig. 10). Eolian facies dominate the mapped upper surface of the Star Town unit, forming a small dune field at the south end of the present-day island, which indicates an east to west dominant transport direction similar to present-day prevailing easterlies (Fig. 9A, B, and C). In addition to the south coast dune–shoreline complex that must represent an embryonic core to the island, there is a distinctive high dome at the northeast terminus of the early-formed dune ridge that is mantled by lower MIS 5e–age material but is likely cored by stage 9/11 strata (labeled *old ridge* in Fig. 9A). This buttress, together with the southern dune complex, represent the pinning points for the first set of east-facing dunes of lower MIS 5e age and must be an early feature, here shown to be MIS 9/11. Along most of the south coast,

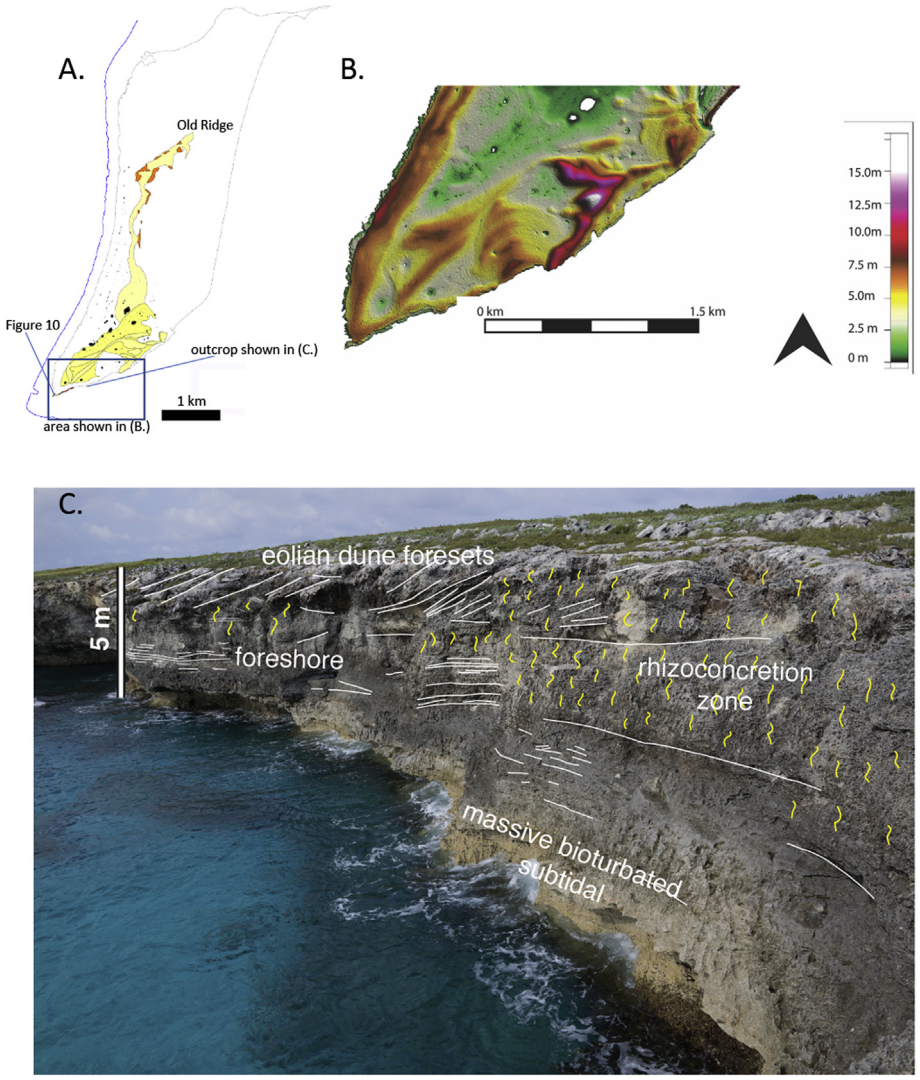

Fig. 9. Star Town unit. (a) Distribution of Star Town unit; (b) bare-earth lidar image of southern portion of West Caicos, showing distinct dune complexes of Star Town unit; (c) vertical facies succession of Star Town unit along south coast showing massive subtidal facies and parallel-stratified foreshore, followed by eolian strata. A well-developed rhizoconcretion zone is developed in crest of Star Town dune.

the top—Star Town surface is capped by an extensively developed 5–10-cm-thick laminar blackened calcrete with blackened clasts and a penetrative rhizoconcretion zone that is up to 2 m thick (Fig. 12). Strata overlying the Star Town unit along the south coast are only a thin (0.5–2 m) veneer of upper MIS 5e grainstones with extensive younger caliche overprint (Fig. 12).

The Star Town unit displays the oldest relative D/L ratios of >0.6 (D/L Glu mean: 0.610 ± 0.028 [N = 9], converted to A/I mean [Whitacre et al., 2017]: 0.814 ± 0.069 [N = 9]). In addition, two U–Th dates from corals of a coral–rudstone washover deposit situated 0.6 km west of Star Town yield ages of 365 and 368 ka ± 5.5 ka (Figs. 7 and 8; Tables 1 and 2). Though these corals are not pristine (note $\delta^{234}U_{initial}$ of 174), both of these dates suggest a middle Pleistocene age. A research borehole taken by Waltz (1988) also intersected a weathered coral facies below MIS 5e reefs at Boat Cove (Fig. 5) that we assume is equivalent to the Star Town unit, though no reliable ages were generated from this core material (Wanless and Dravis, 1989; Kindler and Meyer, 2012).

Projection of a north-trending arm of Star Town carbonates along the west side of Lake Catherine is made on the basis of karst sinkhole density along this low-relief interior zone (Figs. 9A and 13). This karst plain connects the southern dunes with the northern buttress. The greater density/abundance of sinkholes is consistent with the older karstified carbonates that have been exposed subaerially, most likely for four glacioeustatic lowstands (the MIS 10, MIS 8, MIS 6 and MIS 2–4). Only in this southern area of West Caicos mapped as the Star Town unit is such a density of sinkholes observed. An unusual set of narrow high-relief ridges isolated within the interior of West Caicos (Figs. 5, 9, 13, and 14A) are interpreted as coastal-beach-barrier ridges marking the Star Town unit shoreline(s) in the middle Pleistocene.

5.1.1. Interpretation

The recognition of a middle Pleistocene age for West Caicos outcrops was suggested by work of Wanless and Dravis (1989, their p. 70.) and further supported by AAR and U–Th work of Kindler and Meyer (2012). Our data support the presence of older strata, but our distribution of this older unit (our Star Town unit) is different than that proposed by Wanless and Dravis (1989). The AAR from the Star Town unit shows D/L Glu >0.6 and the two U–Th dates on corals of

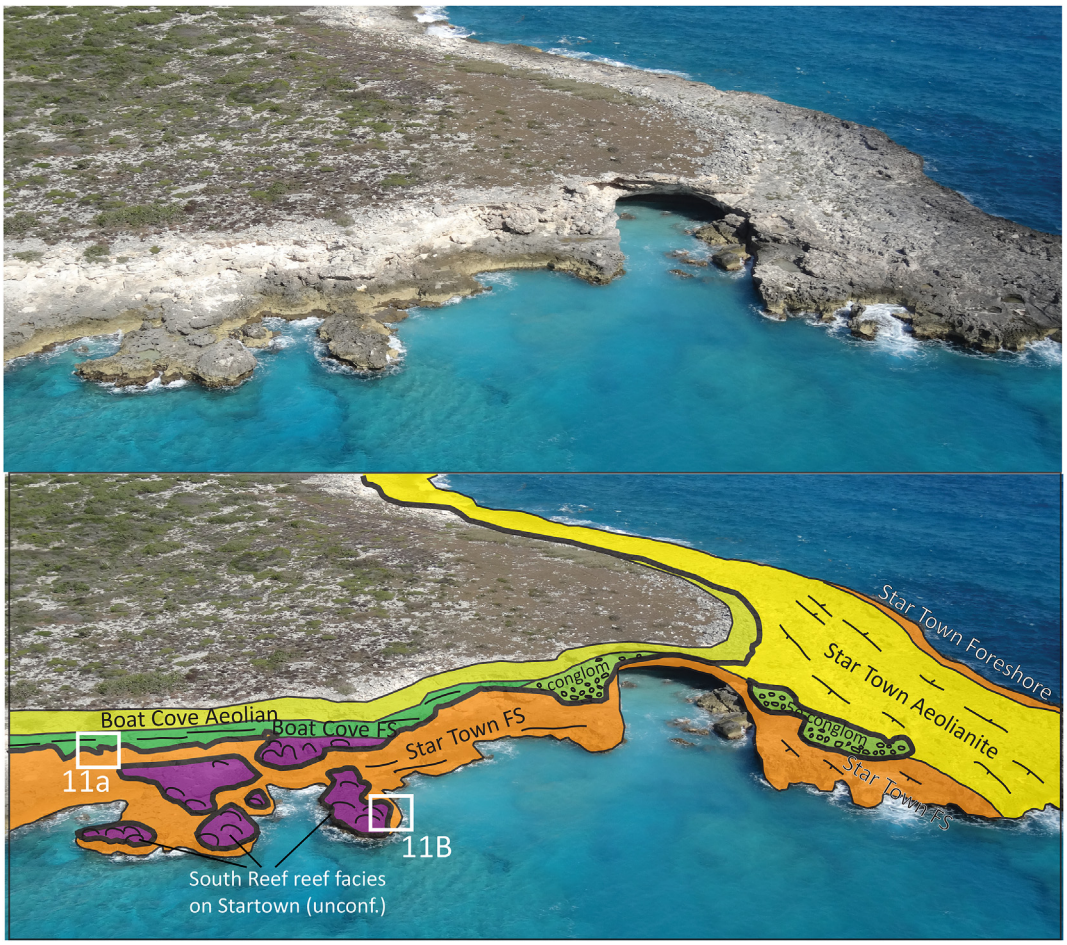

Fig. 10. Star Town/South Reef unconformity at Southwest Point. Both eolian and foreshore facies of Star Town unit are present at southwest tip. Reef and foreshore facies of South Reef unit onlap and encrust eroded Star Town unit. Dips on Star Town foreshore beds are to north on north side of point, and to south on south side of point, illustrating the original MIS 9/11 origin of this southwest promontory. See Fig. 9 for location. Highlight boxes are detailed in Fig. 11.

365 and 368 ka, as well as the extensively developed *terra-rossa* paleosol capping in this unit, strongly favor a middle Pleistocene stage 9 or 11 deposit. Kindler and Meyer (2012) provide data from a research borehole near Boat Cove that also support the presence of middle Pleistocene in the shallow subsurface along the west coast of the island. The detailed paleogeography established for the Star Town unit (Fig. 14A) is among the most detailed of any available in the BTC chain for this age strata. Mid-Pleistocene units have been documented from several islands including San Salvador (Hearty and Kindler, 1993), Eleuthera (Kindler and Hearty, 1995, 1996; Hearty, 1998), New Providence (Garrett and Gould, 1984; Hearty and Kindler, 1997), and Bermuda (Vacher et al., 1989; Hearty and Vacher, 1994; Hearty, 2002; Rowe and Bristow, 2015), as well as more recently in the nearby Great Inagua platform (Kindler et al., 2007; Thompson et al., 2011) and Mayaguana (Kindler et al., 2011; Godefroid, 2012). However, as mentioned earlier, the degree of preservation of facies and ability to use lidar to map unit distribution greatly improves our ability to reconstruct this stage of island evolution. The Star Town unit established a southern nucleus for the island that subsequently built northward and eastward.

5.2. LIG units: Railroad Ridge, South Reef, boat cove, and Northeast Ridges

5.2.1. Railroad Ridge unit

The Railroad Ridge unit is the earliest-formed north–south linear dune ridge set on West Caicos and is best exposed along a set of cuts on an old railroad grade near the middle of the geomorphic element, thus the unit designation (Fig. 5). The Railroad Ridge unit is 4 km long and 50–100 m wide, with an average elevation of +7 m and several small peaks that reach +11 m. A well-developed calcrete mantles the top of the western dune ridge as well as the next ridge to the east, but no evidence of karst sinkholes such as those developed atop the Star Town unit are observed. The Railroad Ridge unit is composed of a mixed skeletal–peloidal grainstone. The mean value of D/L Glu is 0.521 ± 0.023 (N = 4) with a converted A/I mean of 0.605 ± 0.049 (N = 4) (Whitacre et al., 2017). This AAR value is intermediate between the 0.63 of the older Star Town mid-Pleistocene and the main 0.45–0.46 of the other MIS 5e units discussed below (Fig. 7A).

5.2.2. South Reef unit

The South Reef unit (Figs. 5, 8, 10, 11, 14 and 15) outcrops on the southern half of the west coast of West Caicos from Southwest Point to just south of Boat Cove, a distance of 5.75 km (Fig. 16). The type area for the South Reef unit displays classic spur and groove structures as well as a well-developed coralline algal reef crest at 1 km north of Southwest Point (Figs. 5, 16 and 17). Detailed mapping in the Southwest Point area demonstrates that the South Reef unit rests unconformably above the Star Town mid-Pleistocene (Figs. 10 and 11). The South Reef unit where fully developed displays a complex mosaic of facies typical of a barrier-to-fringing reef

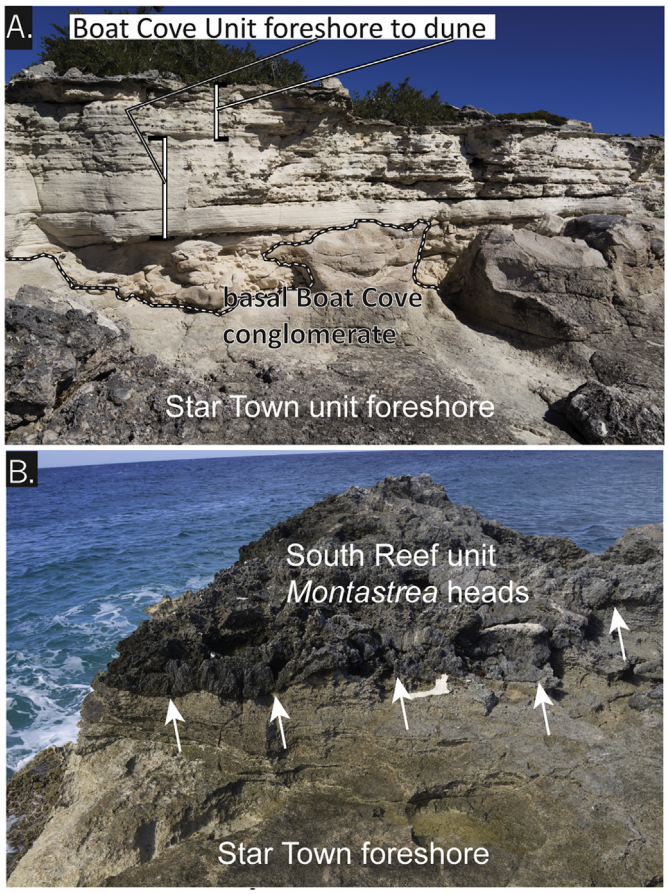

Fig. 11. (a) Sculpted, wave-eroded unconformity separating Star Town foreshore grainstone below from minor conglomerate and foreshore grainstone of Boat Cove upper MIS 5e unit above; and (b) South Reef lower MIS 5e coral heads nucleating on eroded foreshore facies of Star Town unit. The knife-sharp unconformity represents an erosional vacuity of approximately 300–200 ka.

system with a frontal zone of *Acropora cervicornis* (Wanless and Dravis (1989); a reef front/reef core of *Acropora palmata* with lesser head corals including *Montastrea*, *Porities*, and *Diploria*; a well-developed coralline algal crestal facies; and inter-reef grooves with grainstone and small patches of head corals (Figs. 16–18). The total thickness of the South Reef unit is best estimated from the Boat Cove–area cores to be approximately 15 m (Wanless and Dravis, 1989; their Fig. 66).

The average age of the South Reef unit derived from 8 well-preserved samples is 126.5 ka (Fig. 8B) and the AAR D/L Glu mean is 0.401 ± 0.018 (N = 6), yielding an A/I mean (Whitacre et al., 2017) of 0.373 ± 0.032 (N = 6). This low AAR value is not predicted by stratigraphic position as overlying Boat Cove unit samples yield distinctly higher (i.e. older) values (0.40–0.47). However, this relationship is not uncommon with certain bioclastic samples.

5.2.3. Pre-boat cove unit erosion and boat cove unit

Deposition of the South Reef unit was terminated by a significant erosional event that resulted in removal of as much as 3 m of the upper portion of the South Reef profile, with erosion increasing northward from the unaffected South Reef area toward Boat Cove where the erosional surface has cut downward from the South Reef elevation of +4 m–0.5 m above present sea level (Figs. 5, 19 and 20). This erosion caused widespread planation of the upper surface of the South Reef unit and truncation or total removal of the crustose coralline algal (CCA) cap seen at South Reef (Figs. 19 and 20). A 0–1.2 m thick coral rubble conglomerate with clast sizes that range up to 25 cm is a diagnostic marker of this erosional event (Fig. 19B and C). The coral conglomerate is mapped across the entire 5.6 km of outcrop of the South Reef unit (Fig. 20) and initially was considered to represent a coral rubble facies contemporaneous with the South Reef complex. More detailed inspection shows that the conglomerate, while thickest in the grooves of the South Reef unit, also extends across spurs and interfingers with basal ooid grainstones of the overlying Boat Cove unit, which possesses a distinctly younger age of 120.6 ka (Fig. 8B). Eroded and wave-polished stands of *A. palmata* directly overlain by foreshore ooid grainstones with rounded cobbles of the coral conglomerate provide further evidence of this through-going erosion (Fig. 19A), as do the truncated erosional remnants of the CCA cap of the South Reef facies (Fig. 19B).

Above the basal conglomerate just considered, the Boat Cove unit consists of scattered coral heads that encrust the basal erosion surface. The basal Boat Cove unit conglomerate is succeeded and buried by a southward-prograding, shore-parallel, offshore–upper shoreface–foreshore dune succession that rims the western coast of West Caicos. This foreshore-eolian facies of the Boat Cove unit also forms a thin cap that rests directly on the Star Town unit along the south coast of the island (Figs. 5 and 23).

A distinct population of post-erosion coral heads and small patch reefs with heads of *Montastrea annularis* (dominant) and *Diploria* (subordinate) are found to occur attached to the top–South Reef erosion surface (Fig. 24). Minor encrustation of coral heads by the coralline alga *Goniolithon* is seen locally, and it is common to see the upper surface of the corals encrusted by *Chama* clams.

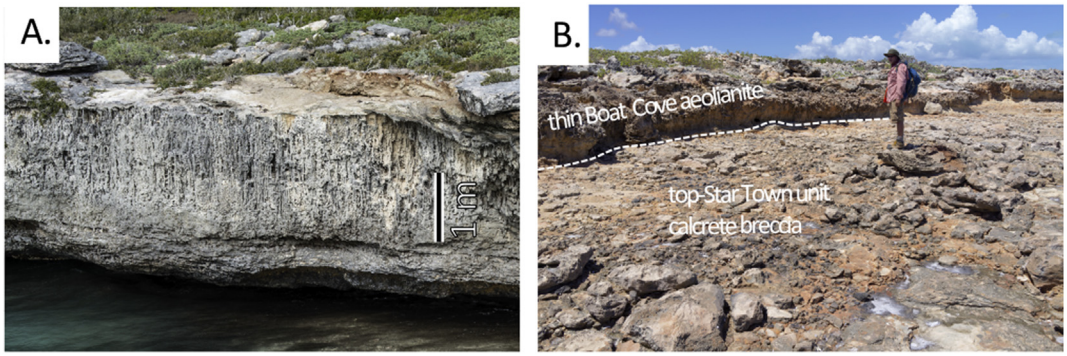

Fig. 12. (a) Star Town eolianites with extensive rhizoconcretion zone marking a prolonged period of subaerial exposure prior to onlap of Boat Cove upper MIS 5e carbonates. (b) Upper surface of Star Town unit displays a widespread and extensively developed calcrete–breccia interval with blackened clasts and breccia blocks lithified into upper surface, with blocks up to 40 cm in diameter. All blocks shown on surface where geologist is standing are mid-Pleistocene, not Holocene.

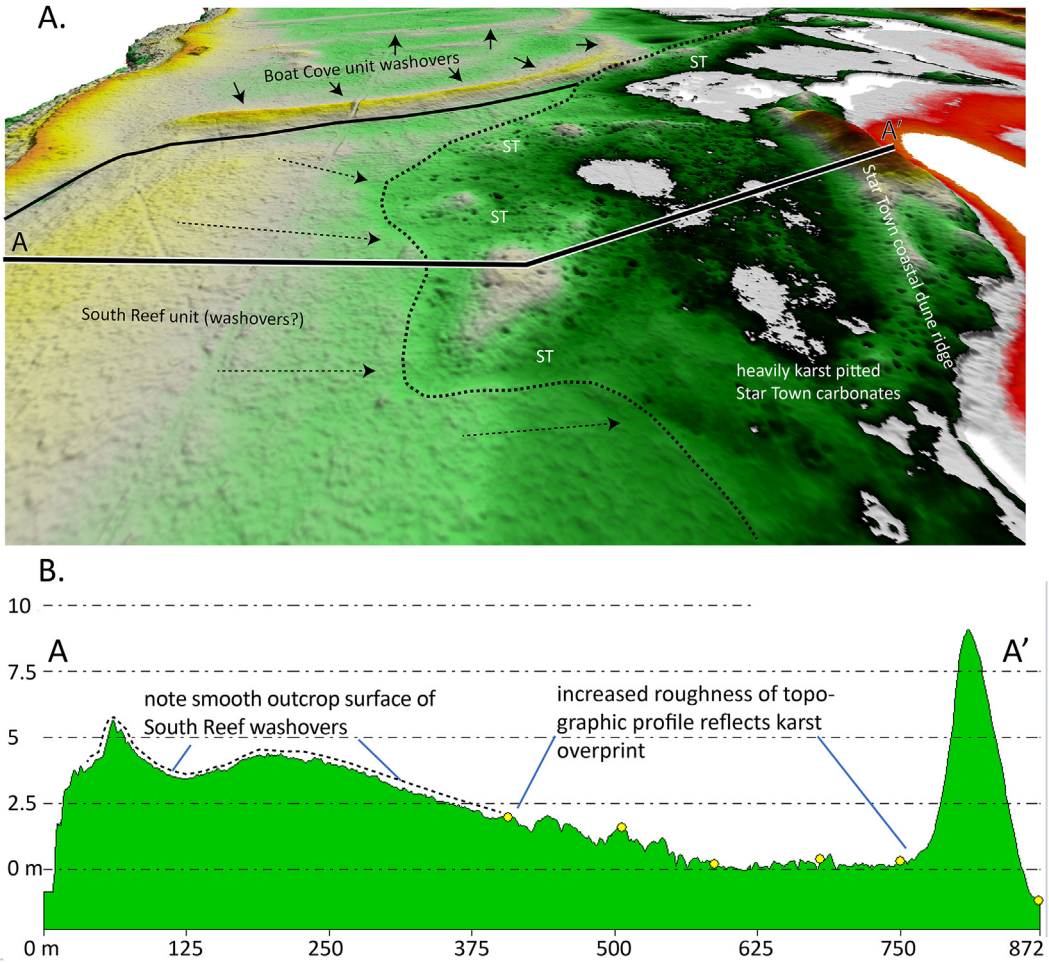

Fig. 13. Karst topography developed specifically on top of MIS 9/11 Star Town carbonates as shown by contrast in upper surface topographic profiles and abundance of sinkholes in older Star Town vs. younger South Reef and Boat Cove units. (a) False-color DEM image from airborne lidar showing pitted upper surface of Star Town vs. MIS 5e carbonates; and (b) topographic profile along A-A′ showing change in surface roughness associated with karst overprint.

Maximum vertical growth of coral patch reefs is 2 m (Fig. 20); individual patches can be 3 m in diameter (Fig. 24A). This phase of coral growth is distinct from the South Reef unit corals in that they show no signs of an erosive upper surface and are buried by ooid sands of the Boat Cove foreshore–upper shoreface in a pristine condition (Fig. 24C). Further, whereas head corals of *Montastrea* and *Diploria* are observed in the South Reef complex, no *A. palmata* or *A. cervicornis* are observed in these post-erosion coral complexes. U–Th dates on these coral heads yield a mean age of 120.5 ka (n = 9), and both the age and occurrence of this second phase of MIS 5e corals compare very favorably to those documented on nearby Great Inagua by Kindler et al. (2007) and Thompson et al. (2011).

Overlying the locally developed post-unconformity coral heads on the west coast of West Caicos (Fig. 20), a 10–50-m-wide belt of back-beach, foreshore, upper shoreface, and subtidal peloid–ooid–composite-ooid grainstones with up to 20 percent skeletal fragments was deposited landward of the sparsely developed coral-patch reef trend (Jones and Awiller, 2008; Danger, 2016). The sedimentology of this unit is best seen at the Boat Cove locality (Figs. 21 and 22), where detailed work by Jones and Awiller (2008) and Danger (2016) (Fig. 22) document a progradational to slightly forced regressive foreshore–shoreface succession with minor coral–red-algal facies at the base. A thin landward-dipping boulder and grainstone washover ridge with less than 2-m relief also parallels the trend of the beach deposits along the west coast and is capped by a well-developed calcrete (Figs. 21A and 22). Paleocurrent analysis using foresets of 10–20-cm-thick trough cross strata within the upper shoreface yield a unimodal north–south transport along the west coast, indicating a northerly source of at least the ooid component of the Boat Cove unit (Danger, 2016).

5.2.4. Northeast Ridges unit

Contemporaneous with the Boat Cove unit and following the South Reef unit, a complex series of dune ridge–strandplain deposits are developed along the north and northeast margins of West Caicos (Fig. 23). The mean D/L values from the strandplain deposits (marine and eolian mix) vary little, with almost all values falling around 0.45–0.46 (Fig. 7). These values also compare closely with values from the Boat Cove unit of the west coast that also fall in the 0.40–0.47 bracket.

Within the Northeast Ridges set on West Caicos, three different styles of deposition are recognized. The earliest of the dune-ridge deposits of the Northeast Ridges set are a set of three semicircular low-relief (1–2-m-high) ridges found in the northwest part of the island between the west coast and the east end of the runway (Fig. 5) and extending from just north of Boat Cove to just 2 km northwest of Lake Catherine (Fig. 23). A limited number of road cuts expose the internal architecture of the ridges, which are typically

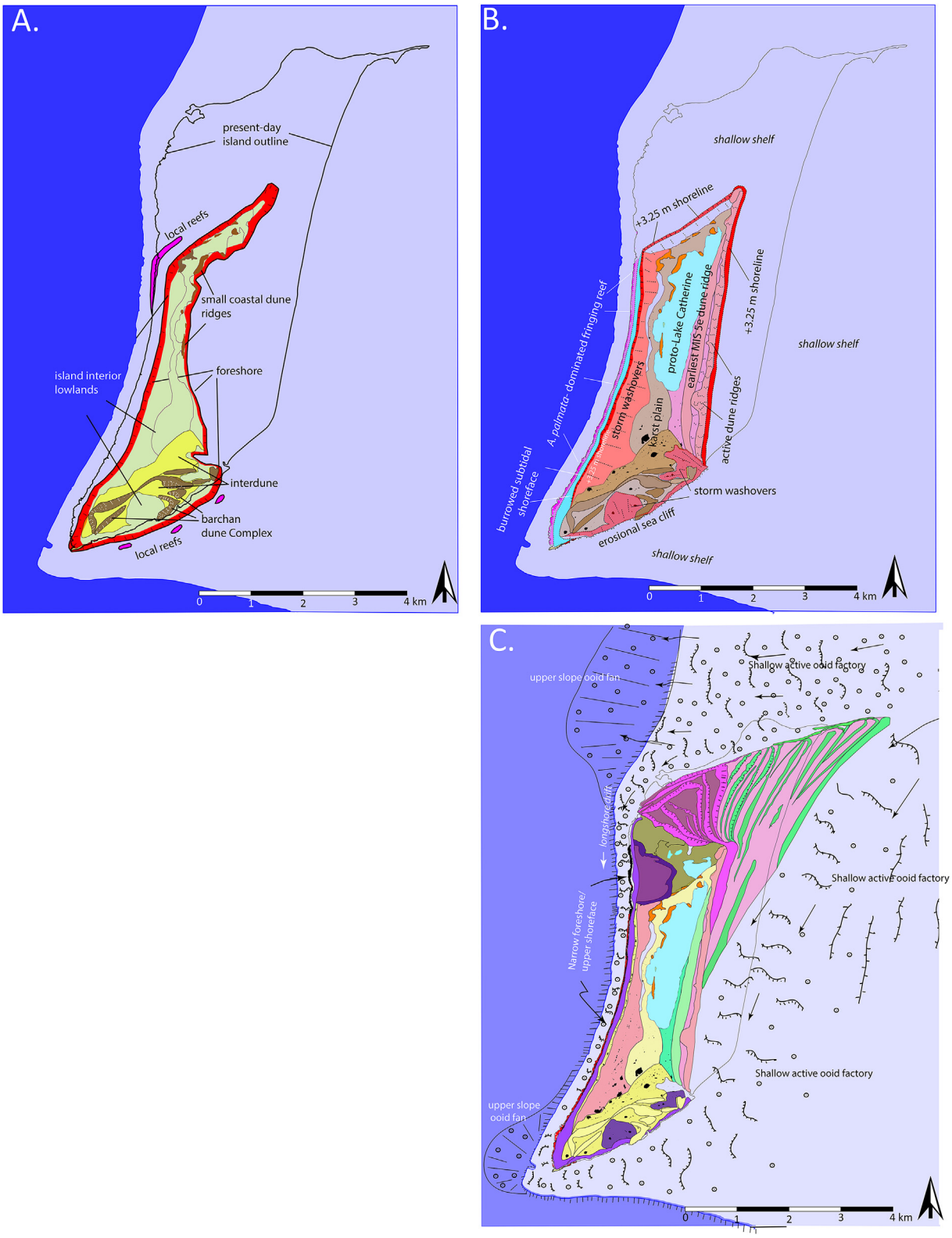

Fig. 14. Paleogeographic maps for MIS 9/11 (Star Town unit), early MIS 5e (South Reef unit), and late MIS 5e (Northeast Ridges set and Boat Cove unit together). (a) Star Town paleogeography with foreshore, local reef development, and eolian ridge complex (tan/brown) on the south coast. (b) South Reef and Railroad Ridge units of lower MIS 5e affinity forming main island core. A continuous fringing reef occurs on the west coast with dune ridges developing in the east. The northern extent of the lower MIS 5e shoreline is shown and is estimated at +3.25 m. (c) Wide-spread ooid deposition occurs during Boat Cove (upper MIS 5e) sedimentation, with the west coast dominated by ooid beaches and the NE expansion of the island into the source of ooid formation. See text for discussion.

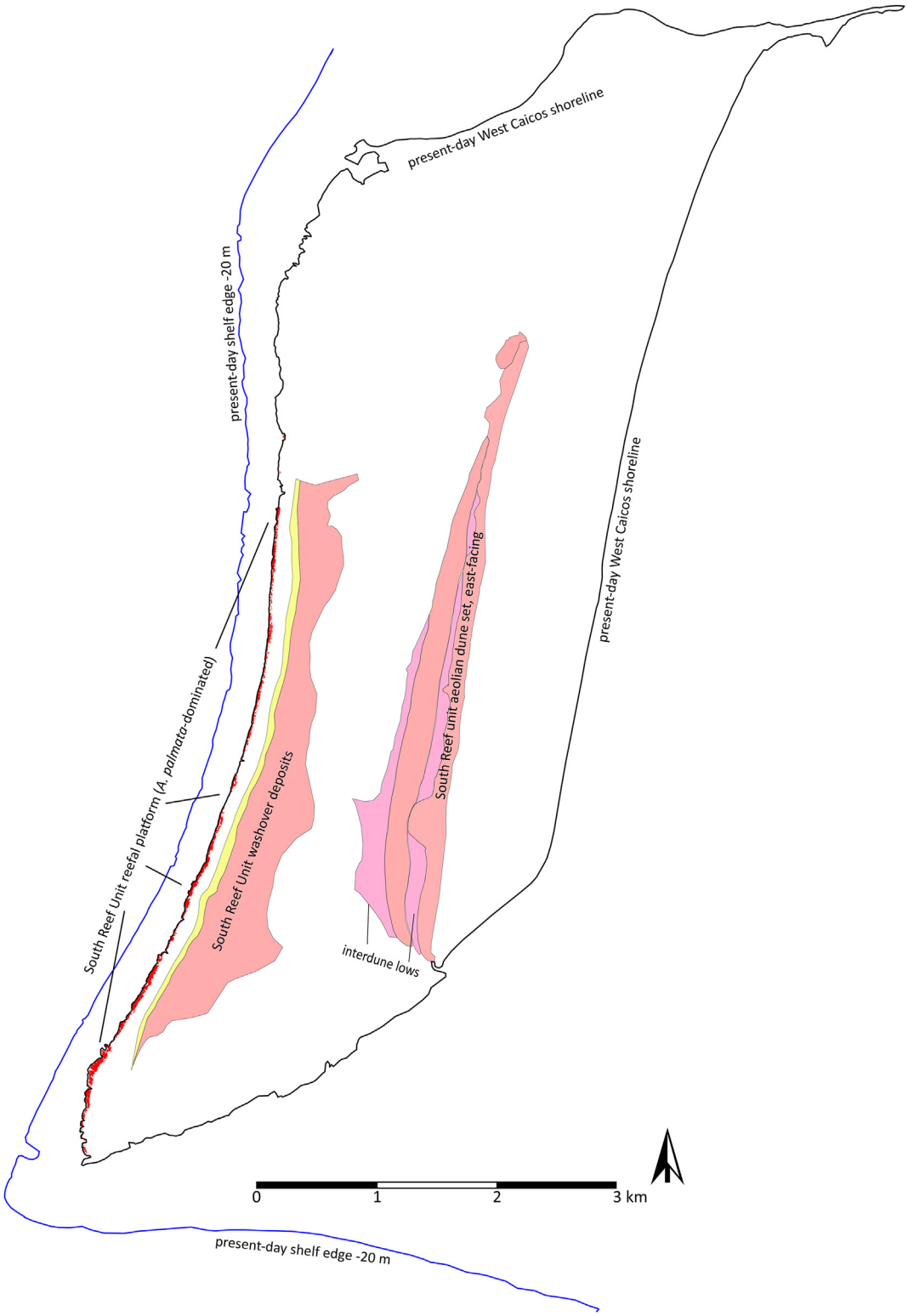

Fig. 15. Map showing distribution of South Reef unit reefal and washover facies along west coast of proto–West Caicos island, and an eastward-accreting dune ridge set on east side of island.

0.5 m in thickness and show low to moderate dipping strata with dips of up to 15°.

A set of three large and two smaller northward- and eastward-accreting dune ridges follows, forming a triangular wedge of ridges up to 16 m high (Fig. 25). These ridges can be mapped continuously to the west shore of the island, where they feed ooid grainstones of the Boat Cove foreshore–shoreface succession by process of longshore drift as documented by paleocurrent data from Danger (2016), with an ultimate source that is speculated to be offshore to the north and east during MIS

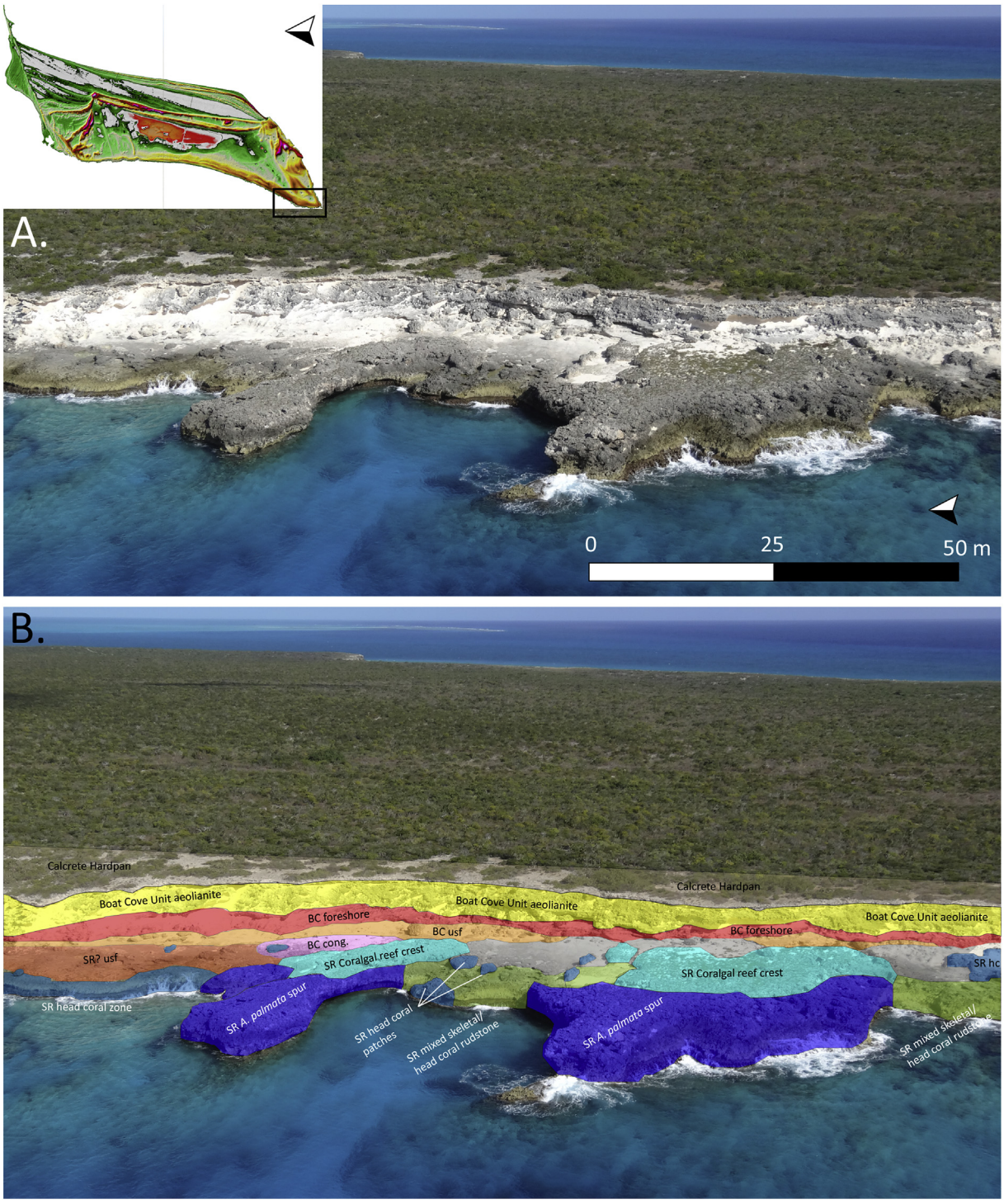

Fig. 16. South Reef unit type outcrop along the southwest coast of West Caicos. Spur and groove architecture of this reef is well developed and illustrates spurs dominantly composed of *Acropora palmata* with a reef-crest facies of crustose coralline algae (mostly *Goniolithon*). (a) Oblique aerial image of spurs; and (b) spur and groove area with facies mapped on model.

5e time. An important aspect of this phase of dune-ridge development is that accretion is equally recorded in northward- and eastward-prograding sets (Figs. 23 and 25). These field relations also demonstrate the contemporaneous nature of the Boat Cove foreshore–shoreface beds and the early ridges of the Northeast Ridges set.

The final phase of dune-ridge accretion associated with the late Northeast Ridges set is the arcuate strandplain set of about seven low ridges forming the east–northeast-pointing tip of the island. Dune ridges are of relatively low relief (1–3 m), and interdune areas are at or slightly below present-day sea level. Viewing a topographic profile cut perpendicular to these ridges illustrates a steadily falling elevation of the "nested" dune ridges (Fig. 25). Along the northeast coast of the island, the foreshore deposits associated

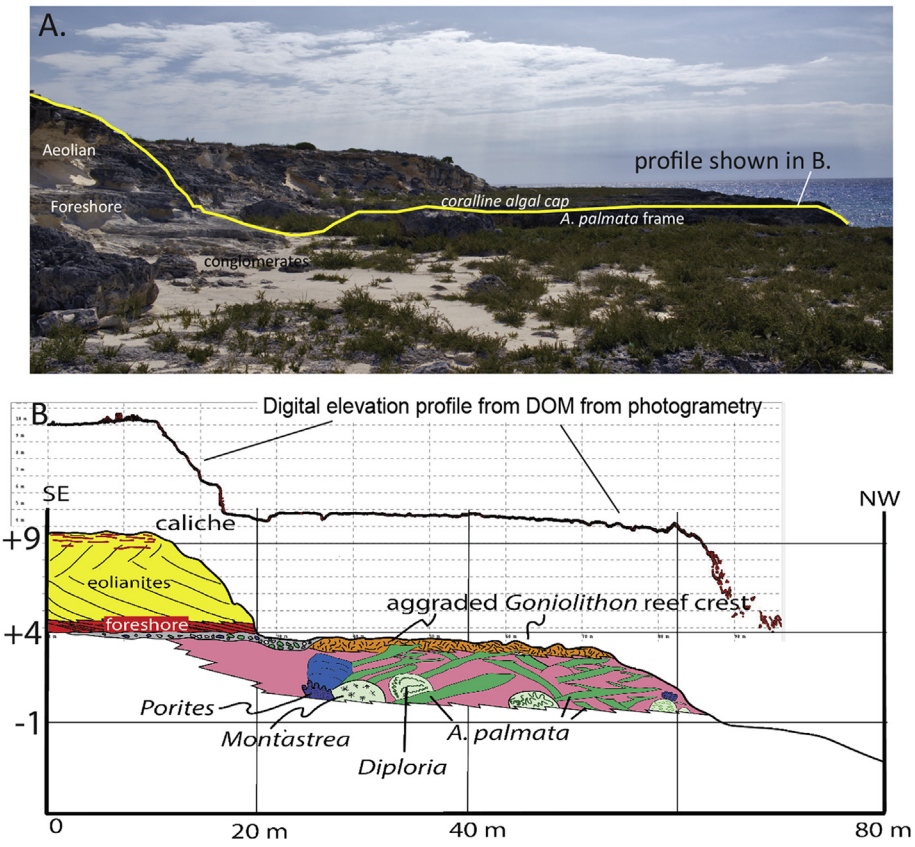

Fig. 17. South Reef unit type outcrop illustrating distinctive flat-topped *Goniolithon* reef-crest facies. Rather than an erosional surface, this growth surface provides a clear estimate of sea level at +3.75 m or slightly greater for lower MIS 5e. Note that foreshore and eolian outcrops on east side of view (left) are of upper MIS 5e Boat Cove unit, separated by a locally developed boulder conglomerate.

with these dune ridges were initially at approximately +4 to +4.5 m near the westerly initiation point and have since stepped down to +0.7 m above present day; the presence of ridges to the far east of the present-day shoreline suggests that sea level continued to fall below present-day levels at the end of MIS 5e time.

5.2.5. Interpretation of LIG (MIS 5e) units

The Railroad Ridge, South Reef, Boat Cove, and Northeast Ridges units are all interpreted to fit within the MIS 5e or LIG highstand on the basis of U–Th ages as well as of AAR relative-age correlations with the absolute dates. The history of LIG deposits is particularly rich on West Caicos.

Wanless and Dravis (1989) suggested that the Railroad Ridge unit represented the nucleus of the island and served to protect the western coast of West Caicos from sediment migrating from the east, allowing reef development on the western shore of the island. Simo et al. (2008) published a date of 219.5 ka ± 2ka for the Railroad Ridge unit, suggestive of an MIS 7 age, one of the few recognized in the Pleistocene stratigraphy of the West Indies or Bahamian Chain. Though there is doubt regarding the U–Th age that was generated from presumably bulk eolian bioclastic grainstones rather than pristine coral material, the fact that similar facies in the next successively younger dune ridge to the east was dated at 136.1 ± 0.8 ka (Simo et al., 2008) suggests a consistent younging relationship as proposed by both Wanless and Dravis (1989) and Simo et al. (2008). Our preferred interpretation of this eolian ridge is that it represents early MIS 5e deposition on the basis of the D/L Glu value of 0.521 being intermediate between the Star Town middle Pleistocene MIS 9/11 at 0.61 and the South Reef at 0.45 (Dl Glu), as well as the U–Th constrained 130–126 ka age. Further, Pascal Kindler (pers. comm.) indicates that petrographically the Railroad Ridge unit best matches an early MIS 5e unit and not MIS 7.

The position of the Railroad Ridge dune on the landward side of the middle Pleistocene Star Town island complex would have made a very difficult setting for deposition of a MIS 7 eolianite considering an accepted maximum sea level at this stage of 10 m below present (see $\delta^{18}O$ trend of Lisiecki and Raymo (2005), their Fig. 1, and various other studies, e.g., Sherman et al., 2014). Noting that the source of sediment for this early-formed ridge was from the east, it becomes very difficult to fit this sediment supply direction with a MIS 7 sea level as the platform top to the east would have been subaerially exposed. On the basis of relative-age position and necessary easterly derived sediment source, we interpret this dune ridge and the dune set to the east as representing early deposits of the LIG (MIS 5e), when sea level would have again flooded the platform top to an elevation of 3–6 m above present-day sea level.

A common characteristic of the LIG record across the Bahamas and Caicos platform is the development of an early reef system at somewhere between +1 and + 4 m above present day sea level (Carew and Mylroie, 1985, 1995; Wanless and Dravis, 1989; Chen et al., 1991; Hearty and Kindler, 1993; Thompson et al., 2011; Godefroid, 2012; Skrivanek et al., 2018). Coral samples from this reef have been dated from San Salvador (Chen et al., 1991) Great Inagua (Thompson et al., 2011; Skrivanek et al., 2018), and Mayaguana (Godefroid, 2012), among other sites, and the range of ages extends from 132 to 117ka. The South Reef unit yields a mean age of 126.5 ka (Fig. 8) and fits this overall model well. Reasonable agreement also exists with sites including the Yucatan Peninsula

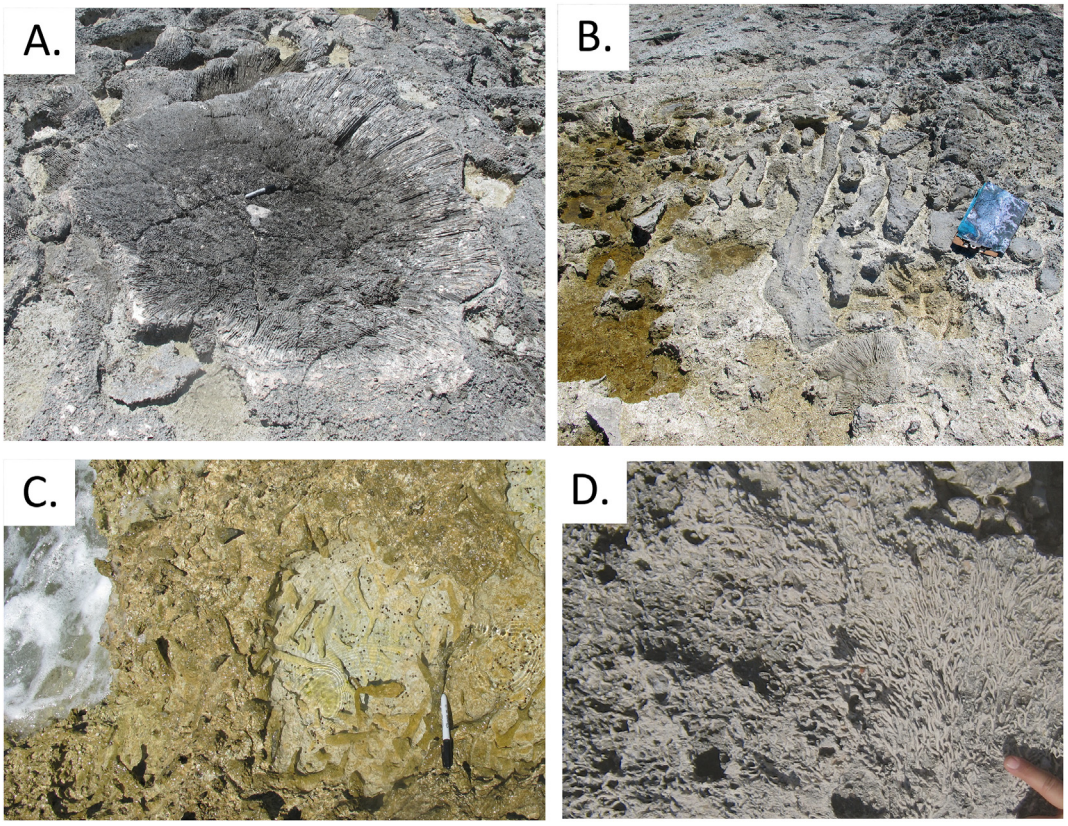

Fig. 18. Characteristic reef builders for lower MIS 5e reef system. (a) *Diploria* head. Marker for scale. (b) In situ stand of *A. palmata* near reef core. (c) Near in situ *A. cervicornis* fragments in low-energy pocket within lower MIS 5e reef. (d) Reef-crest *Goniolithon* boundstone, characteristic of upper 0.5–1 m of lower MIS 5e reef.

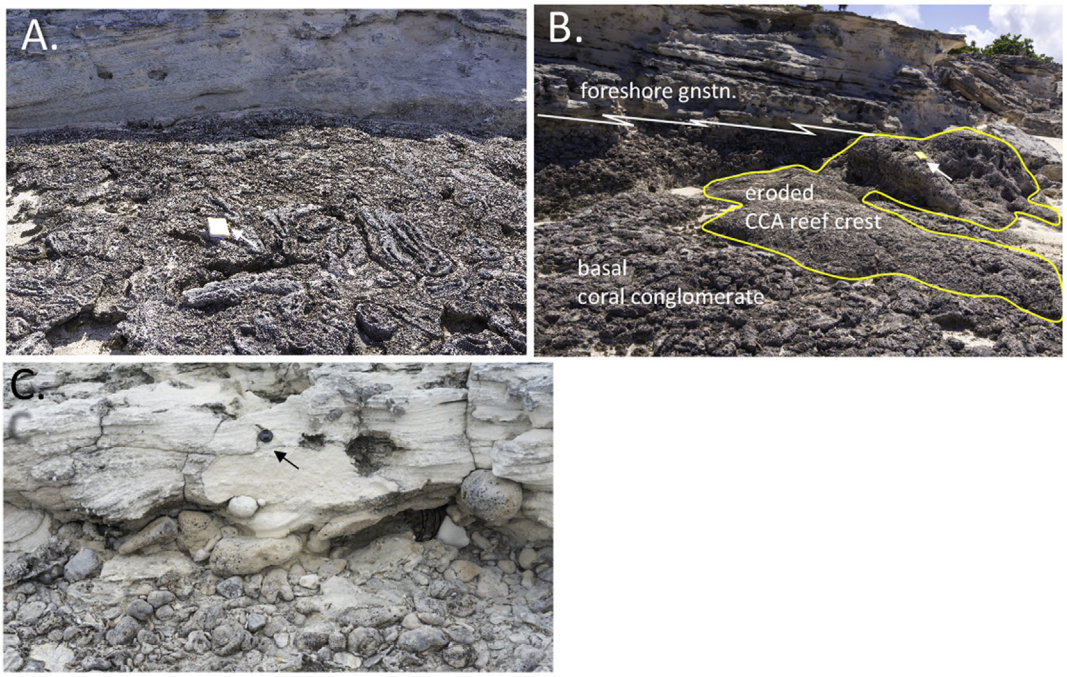

Fig. 19. Examples of intra-MIS5e unconformity. (A) *A. palmata* stand that is planed off erosionally and then overlain by ooid grainstone facies of upper MIS5e Boat Cove unit. Field notebook for scale is 16 cm long. (B) Erosional remnants of coralline algal reef cap of South Reef unit overlain by coral conglomerate and finally by foreshore grainstones of Boat Cove Unit. (C) Detail of coral conglomerate overlain by Boat Cove unit foreshore deposits. Lens cap for scale is 55 mm diameter.

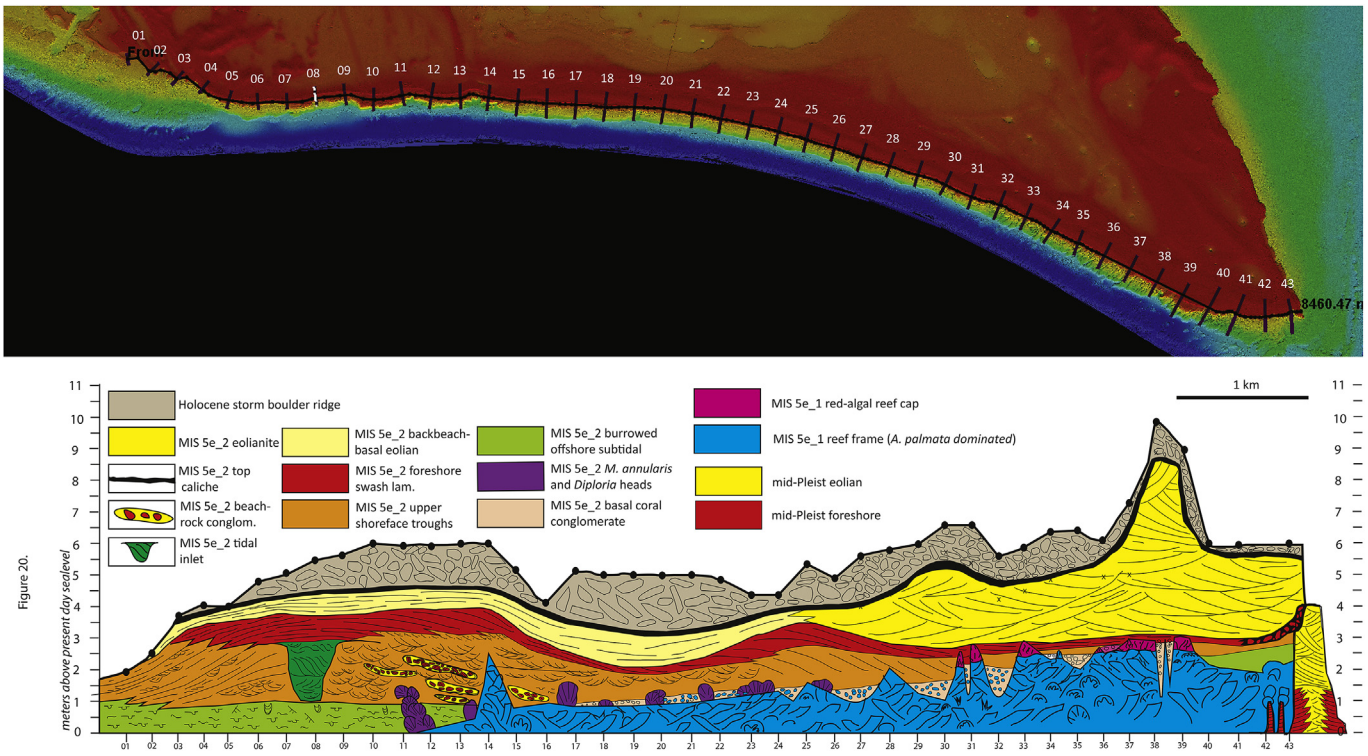

Fig. 20. (a) Stratigraphic cross section of west coast of West Caicos generated by taking topographic profiles (from UAV data) perpendicular to shoreline of West Caicos, spaced every 200 m, from the north to the south end of the island. (b) Depositional facies, taken from geologic map after a height of each facies at each profile was generated, were then combined into a collapsed 2D cross-sectional view.

(Blanchon et al., 2009) and far-field sites like Southern and Western Australia (O'Leary et al., 2013; Murray-Wallace, 2018).

The flat upper surface of the reef-crest coralline algal zone highlighted in Figs. 16 and 17 is interpreted to have formed in shallow-water depths as a normal shallow subtidal to intertidal facies similar to that described by Adey (1978) for the coralline algal-reef crest facies from St. Croix and also well-known from modern Pacific "boiler reefs." This surface shows no evidence of being formed by erosional processes as no coral or coralline algae show signs of truncation, and we do not interpret the development of a coralline algal cap as a sign of a drowning phase. Instead, we assume the top of the coralline algal cap to be close to sea level, creating a "pavement" on the reef crest, much like present-day barrier systems. Examining the digital-elevation profile from the South Reef (Fig. 17), one can deduce a sea-level elevation of +4 m, assuming that the coralline algal cap was likely in water depth of less than 1 m (Adey, 1978). It is important to note that the well-preserved flat CCA pavement exists only in the South Reef area (sections 36-40 on Fig. 20). As one moves northward, erosional truncation of the cap is well documented such as near sections 30-31 (Fig. 19B).

The next stage in the evolution of the MIS 5e record on West Caicos is a period of significant erosion of the South Reef complex, as witnessed along the west coast outcrops. This erosion removes as much as 3 m of reef-crest and reef-front section, with the degree of erosion increasing as one follows the contact northward from the type South Reef locality toward Boat Cove (Figs. 20, 21, 23 and 24). Northward, the CCA cap of the reef is progressively stripped off (Fig. 19B); subsequently, the erosion surface incises in situ stands of *A. palmata* on spur crests (Fig. 19A), eventually creating an even surface of erosion or terrace that is positioned just 0.5 m above present-day sea level (Fig. 24A). The abrupt downcutting of reef fabrics and deposition of a coral-rubble conglomerate indicates an increase in the erosive power of waves that would be driven by a lowering of wave base. Support for this lowered base level is found in several localities along the west coast where the foreshore–to–plunge zone transition (basically low-tide marker) in overlying upper MIS 5e Boat Cove grainstones occurs topographically below the crest of the South Reef crest, demanding a minimum lowering of sea level of at least 2.5 m. It is important to note that Wanless and Dravis (1989) proposed that the erosional contacts between the lower reef and overlying ooid units was local and not reflecting any significant time break. Unfortunately, their relationships compare coral to ooid transitions both north and south of Boat Cove. This illustrates that Wanless and Dravis (1989) did not recognize the presence of two distinct coral assemblages, those that are under the major erosion surface that date at 126.5 ka and those above the erosion surface that have an average age of 120.6 ka. Our extensive mapping of these outcrops as shown in Fig. 20 demonstrates this differentiation. We are in complete agreement that the younger, northern corals are buried by ooids that were contemporary. Our field mapping differs however when it comes to the southern reef outcrops where we show clearly that substantial truncation separates these (Fig. 19A). Rather than suggest that these are two different representations of the same contact, we interpret these relationships as separated by several thousand years and a significant period of erosion.

Following the interpreted sea-level lowering and erosion of the early MIS 5e South Reef unit, sea level increased once again to a position approximately +4 m above present. Early colonization of the unconformity surface by isolated coral heads and small patch reefs occurs along the coast from sections 11 through 26 (Fig. 20). These corals display a mean U–Th age of 120.6 ka, bracketing the onset of the second phase of sea-level rise within the LIG. During this second stage of deposition, ooid production became extensive

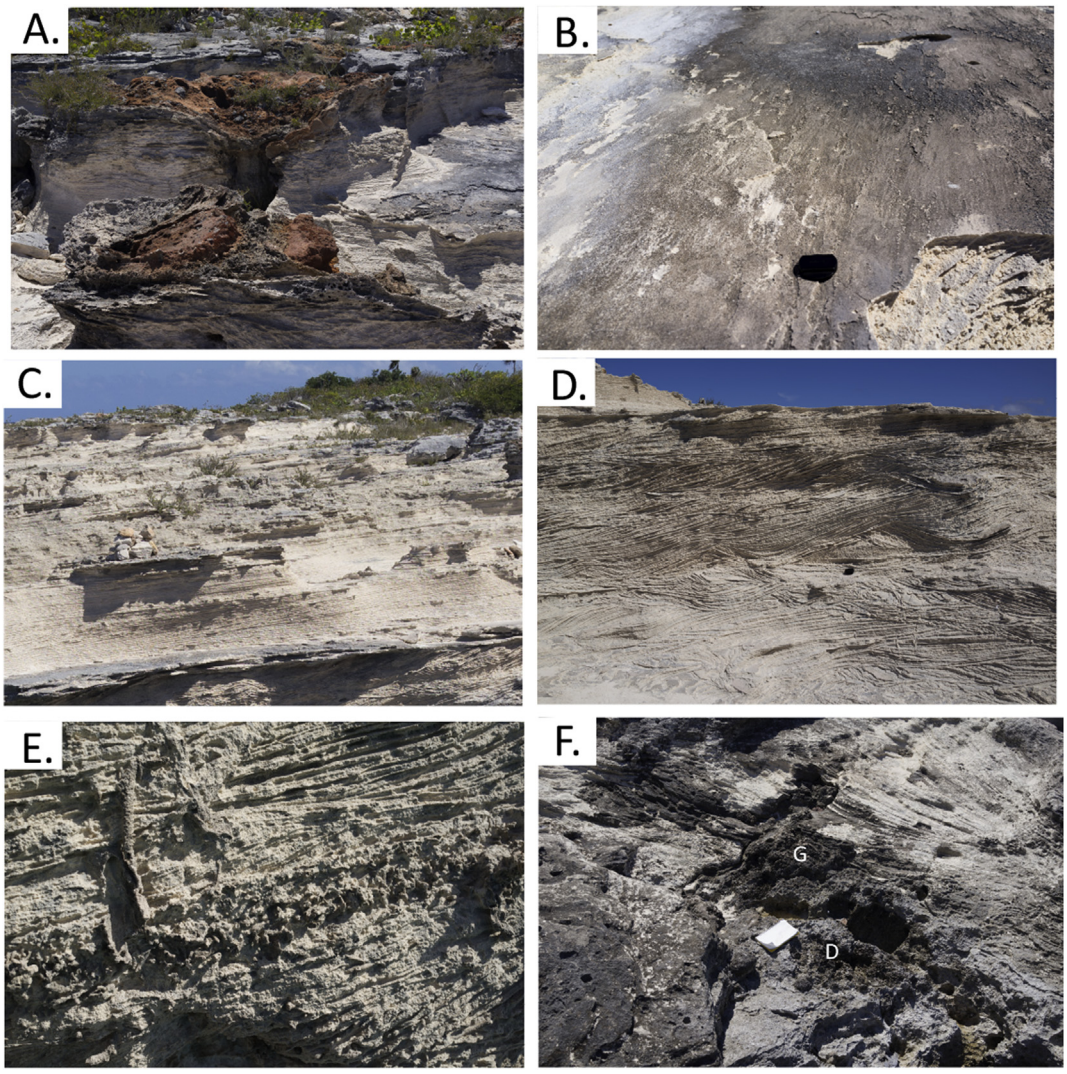

Fig. 21. Representative facies photographs of Boat Cove unit or upper MIS 5e as seen at Boat Cove. Shown in order going down stratigraphic section. (a) Deep red calcrete hardpan with blackened clasts capping Boat Cove unit foreshore grainstones. Field of view (FOV) = 2 m. (b) Parting lineations on foreshore bedding plane. Lens cap is 55 mm. (c) Seaward-dipping foreshore "swash" lamination resting gradationally above upper shoreface trough cross-stratified ooid grainstone. (d) Trough cross-stratified skeletal–ooid grainstone of upper shoreface. View is looking north. All transport directions are southward toward viewer. Lens cap is 55 mm. (e) Burrowed subtidal ooid–skeletal grainstone and grain-dominated packstone in lower part of upper shoreface. Horizontal view is 40 cm. (f) Coral boundstone (HC = head coral) with (g) *Goniolithon* cap at base of Boat Cove section showing presence of early transgressive upper MIS 5e reef development. Field book is 16 cm.

and an aerially widespread series of skeletal–ooid dune-ridge complexes developed, creating both the sediment for the north–south-prograding Boat Cove unit along the west coast and the Northeast Ridges unit that built the island northward, northeastward, and to a lesser extent eastward (Fig. 23). Ooid dune-ridge height decreased progressively as the ridges prograded north and east, eventually stepping below present-day sea level before latest MIS 5e deposition ended when sea level dropped below the platform top (Fig. 25). This pattern matches well with the subtle forced-regressive pattern observed in the Boat Cove unit at Boat Cove and along the west coast of the island (Fig. 22).

5.3. Holocene strandplain and coastal dune deposits

To complete island depositional patterns, Holocene depositional patterns are summarized here. Holocene sedimentation on West Caicos includes two discrete dune ridge–strandplain units on the north and east coasts of the island, as well as one extant (Great Salina) and one relict salina (Company Point Salina) (Wanless and Dravis, 1989) (Fig. 26). Lake Catherine is the main water body on the island and is a near-normal-marine salinity "lake" that is plumbed to the ocean through solution-widened fractures and caves (Wanless and Dravis, 1989; Guidry et al., 2007; Jones and Awiller, 2008). No work on the Lake Catherine sediments has been undertaken; coring and detailed descriptions of the salina fills were carried out by Wanless and Dravis (1989) and by Morgan (2008) but are not considered further here.

Lloyd et al. (1987) documented that the range of ages for the Holocene ooid strandplain–dune ridge complex on the east coast of West Caicos formed between 3450 and 790 ybp (radiocarbon ages on ooid grains). These radiometric ages bracket a narrow D/L Glu mean of 0.219 ± 0.017 (N = 19) and converted A/I mean (Whitacre et al., 2017) of 0.122 ± 0.017.

The eastern dune-ridge complex extends 8 km north–south and is between 20 m and 500 m wide, with approximately six ridges building from +1 m to +6 m (locally up to +12.5 m along the southeastern coast near the erosional limit of the dune ridge) (Fig. 26). This dune-ridge complex on the east coast was more

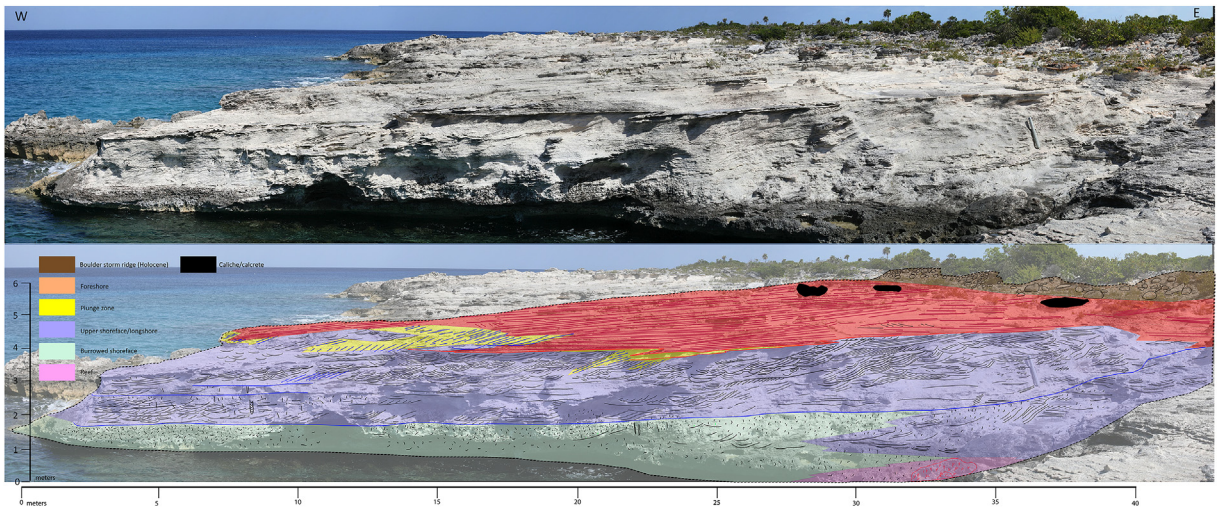

Fig. 22. Detailed facies map of south-facing exposure of upper MIS 5e Boat Cove unit at Boat Cove. Note both the progradational arrangement of facies as well as a minor forced-regressive architecture (downward stepping of base of foreshore from 4.5 m at east to 4 m at west).

active earlier in the Holocene, as evidenced by the progradational pattern that has now become extensively vegetated and stabilized dune ridges. Holocene strandplain ridges on the north-central coast of the island have prograded as much as 1 km. These strandplain ridges have roughly 0.5 m relief; individual ridges are spaced at 50–80 m with an elevation +1 to +1.8 m. The smaller and shorter-spaced northern ridges reflect that the main wind-driven energy, which is the easterly trade winds, is absorbed by the east-facing coastline. During most of the Holocene, the southern and western coasts of West Caicos are bypass or erosional profiles with no net accumulation. This pattern of northerly and easterly accretion during the Holocene matches well with that since the middle to late Pleistocene.

6. Discussion

6.1. Application of lidar and UAV data for pleistocene stratigraphic analysis

One of the key advances from the West Caicos data set derives from demonstrating the value of lidar and UAV-based high-resolution DEM for improved mapping and delineation of Pleistocene morphostratigraphic elements. These data sets have greatly enhanced the ability to interpret and quantify landform development and relative age of units. We illustrate through these data sets that documenting the geomorphology of the islands and its link to island stratigraphy is critical to better constrain the age and understanding of processes of deposition, as well as relative eustatic position of the units involved. In particular, bare-earth lidar imaging of moderately to heavily vegetated islands such as those of the Bahamas and British West Indies (BTC) is shown to be instrumental in highlighting geomorphic features including strandplain patterns, karst development (and thereby relative age of units), dune-ridge accretion patterns, cross-cutting of ridge complexes, and presence and geometry of washover deposits. DEM-based topographic profiles (e.g., Figs. 13, 17, 25 and 26) can be used to highlight unit surface expression styles as well as for documenting systematic changes in beach-ridge elevation, useful for tracking patterns of sea-level change.

One of the important aspects of the development of West Caicos during MIS 5e is the increase in the rate of accretion of the island associated with the upper MIS 5e highstand. This accretion of ooid strandplain ridges can be best observed in the lidar-guided map of the island; the area of expansion can be quantified, highlighting the importance of this event (Fig. 27). On West Caicos, 56 percent of the current island surface is formed by ooid-dominated dune-ridge and strandplain deposits of the upper MIS 5e that were deposited between 120 and 116 ka. When compared to the 16 percent for early MIS 5e, 16 percent for the Holocene, and 12 percent for MIS 9/11, the anomalous sediment pulse is conspicuous. Volumetric comparisons are the more meaningful test of sediment accumulation rates because they incorporate area multiplied by thickness (actual sediment volume), but such volumetric estimates are more challenging as thicknesses are not known for the entire system but can only be observed locally, and are thus less well constrained than area estimates. Whereas the upper surface of accumulation is very well controlled by the lidar-based DEM, the base of each unit is difficult to constrain. For this discussion, we consider the sediments preserved from the base of the foreshore to the top of the depositional surface. For the Holocene, we use sea level as the base of Holocene foreshore and thus generate a sediment volume of 5.02×10^6 m^3 over the last 3400 yr (age control from Lloyd et al., 1987). We assume the Holocene record to provide maximum accumulation rates as virtually no surface weathering has occurred to reduce the sediment volume.

Generating an estimate of sediment volume for the MIS 5e interval requires that a dynamic (ie can't be a fixed elevation) basal surface of the foreshore be used in order to mimic the falling base level during this depositional phase (Fig. 25). For the early part of the upper MIS 5e, when sea-level was estimated at +5 m, we used a +4 elevation, placing the base of the foreshore about a meter below the maximum SL stand. For youngest MIS 5e strand ridges in the northeast part of the island, where foreshore elevation was just +1 m, we used an elevation of 0 m or present sea-level. For the intervening dune-ridge-strand elements, a linearly interpolated elevation was applied (somewhere between +4 and 0 m relative to present-day SL). For the roughly equivalent time span of 3000 yr, the upper MIS 5e record is estimated to have generated between 6.5 and 8×10^6 m^{3}with the uncertainty stemming from the positioning of foreshore elevation.

Regardless of uncertainties in estimates, the difference between MIS 1 (5.02×10^6 m^3 over the last 3 to? 4 ka) and between 6.5 and 8×10^6 in 3 ka for upper MIS 5e represents a 23–38 percent difference in rate of sediment production/preservation. Factoring in

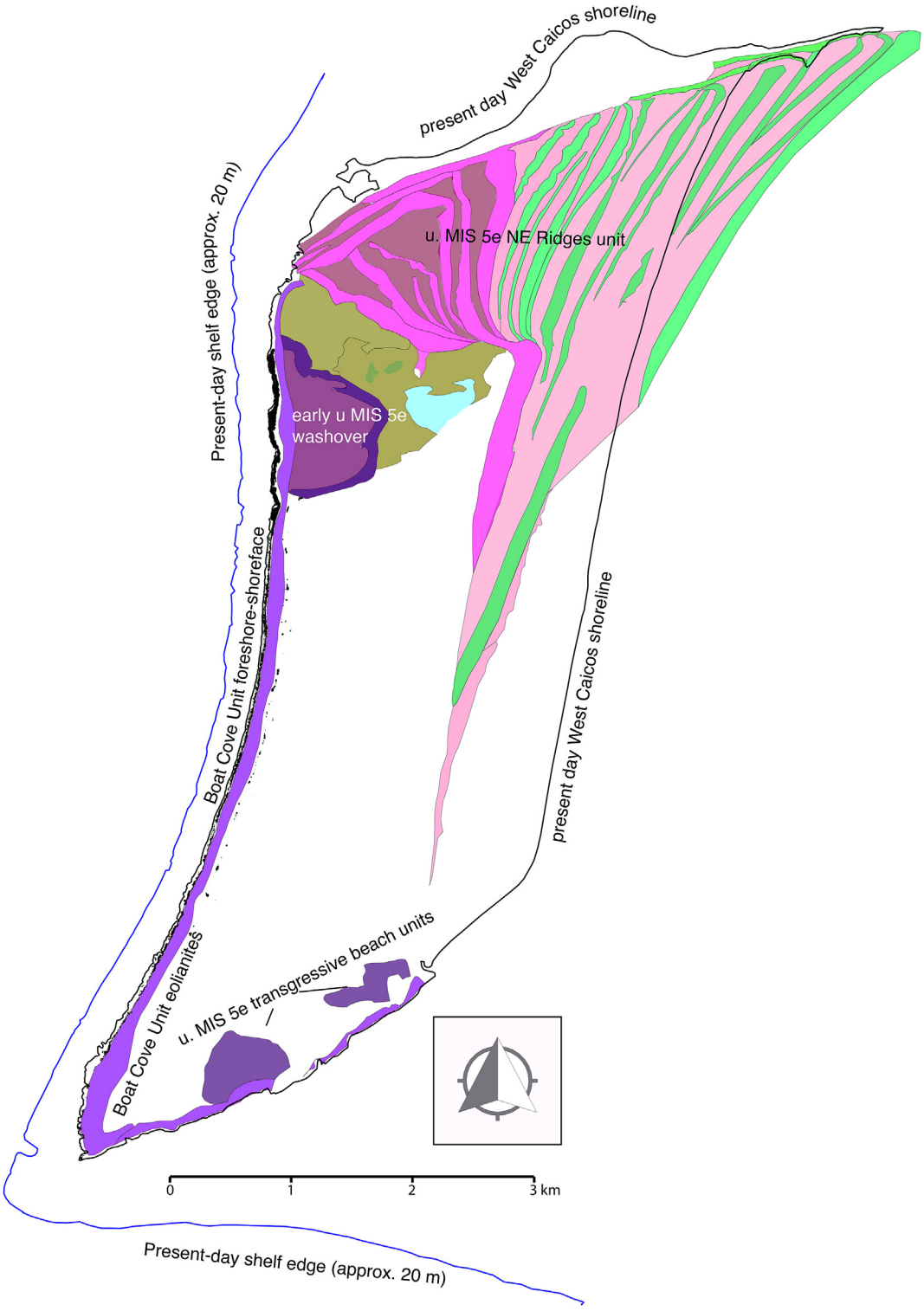

Fig. 23. Facies map of units for upper MIS 5e including Boat Cove unit and Northeast Ridges unit. Refer to geologic map in Fig. 5 for facies/unit key.

the amount of weathering and associated loss of volume for the upper MIS 5e section over the past 120 ka, this difference should be considered a minimum estimate. This increase is rate of accumulation we believe to be representative of many of the islands of the Bahamas and Caicos platforms.

The UAV-generated DEM and imagery served as an ideal base map for capturing the remarkably detailed stratigraphy observed along the west coast of West Caicos (Fig. 6). Field mapping utilizing the UAV-generated base map allowed us to recognize the top MIS 9/11 surface and the intra-MIS 5e unconformity, both surfaces having been unrecognized previously despite the focused studies of Waltz (1988) and Wanless and Dravis (1989), as well as dozens of field trip groups that have visited the area. Estimating sea-level highstand positions and the minimum intra-MIS 5e sea-level-fall erosion-

Fig. 24. Examples of early upper MIS 5e transgressive coral heads. (a) View looking north along west coast of West Caicos approximately 1 km south of Boat Cove (profile 17 of Fig. 20). This view shows the erosional top surface of South Reef unit overlain locally by *Montastrea* bioherms of basal transgressive element of Boat Cove unit. (b) Head of *Diploria* resting unconformably on eroded top–South Reef unit surface. (c) Diploria head in lower part of Boat Cove unit that is overlain with total preservational, nonerosive contact by ooid grainstones of Boat Cove upper shoreface. Contrast this with the strongly erosional contacts observed where Boat Cove grainstones overlie corals of older South Reef unit (e.g., Fig. 19A).

surface topography was? also greatly aided by the reconstructed profiles from the west coast data sets. The resulting constrained cross-sectional panel (Fig. 20) allows confident assessment of the elevation of the lower MIS 5e South Reef elevation—not only at one isolated spot but also as a three-dimensional surface that can be matched to significant reef subfacies such as the crestal CCA caps at South Reef (Fig. 17).

6.2. LIG sea-level record on West Caicos

Characterizing the intra-MIS 5e sea-level change record is an important starting point for improved understanding of climate-change rates and the existence of non-Milankovitchian eustatic fluctuations. Significant data and a range of interpretations exist, aided by the detailed oxygen isotopic records with constraints from coral ages (Shackleton, 2000; Waelbroeck et al., 2002; Lisiecki and Raymo, 2005. The Hearty et al. (2007) synthesis of LIG sea-level history focused attention on the global nature of the intra-5e sea-level fall and presented evidence from Bermuda, the Bahamas, the Mediterranean, and Western Australia that supported an initial sea-level rise to +2 to +3 m, followed by a fall to roughly present-day sea-level, in turn followed by a second brief rise to +3 to +4 m and then a sharp rise to between +6 and + 9 m (Fig. 3). The Kopp et al. (2009) probabilistic analysis of the MIS 5e sea level focused mainly on the magnitude of the 5e sea-level rise (80 percent probability of a +8 m rise during 5e); their analysis appears to show an intra-5e sea-level fall (their Fig. 4a; our Fig. 3C), although this element of their analysis was not discussed in detail. In a later paper

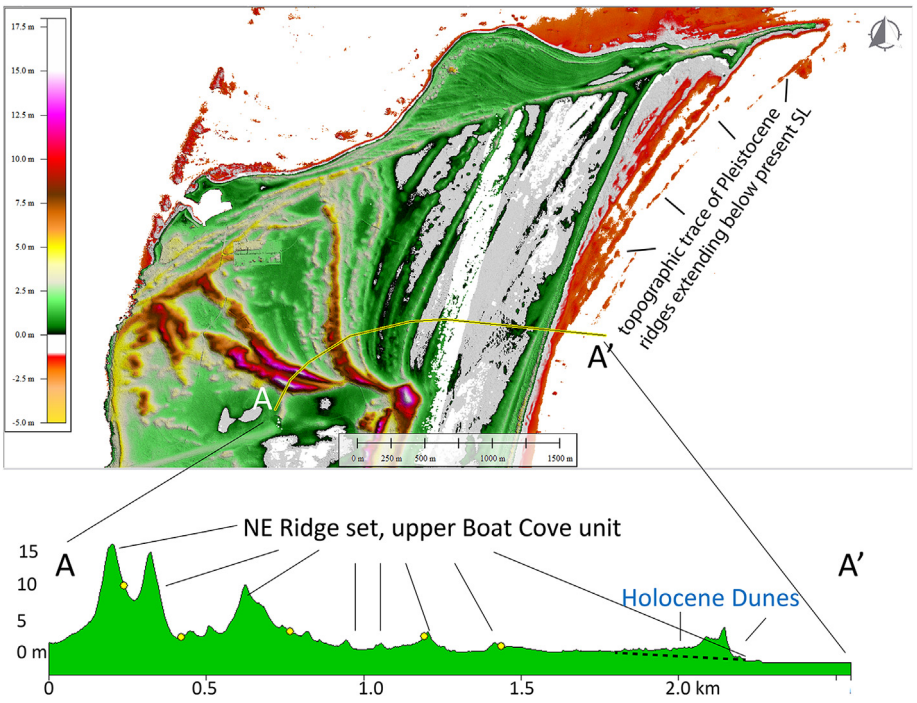

Fig. 25. Lidar-based elevation model of northern portion of West Caicos highlighting eastward-prograding strandplain complex associated with upper MIS 5e Northeast Ridges systems. Crest of dune ridges drops progressively in elevation from approximately 15 m in earliest upper MIS 5e to faint ridge traces below present-day sea level.

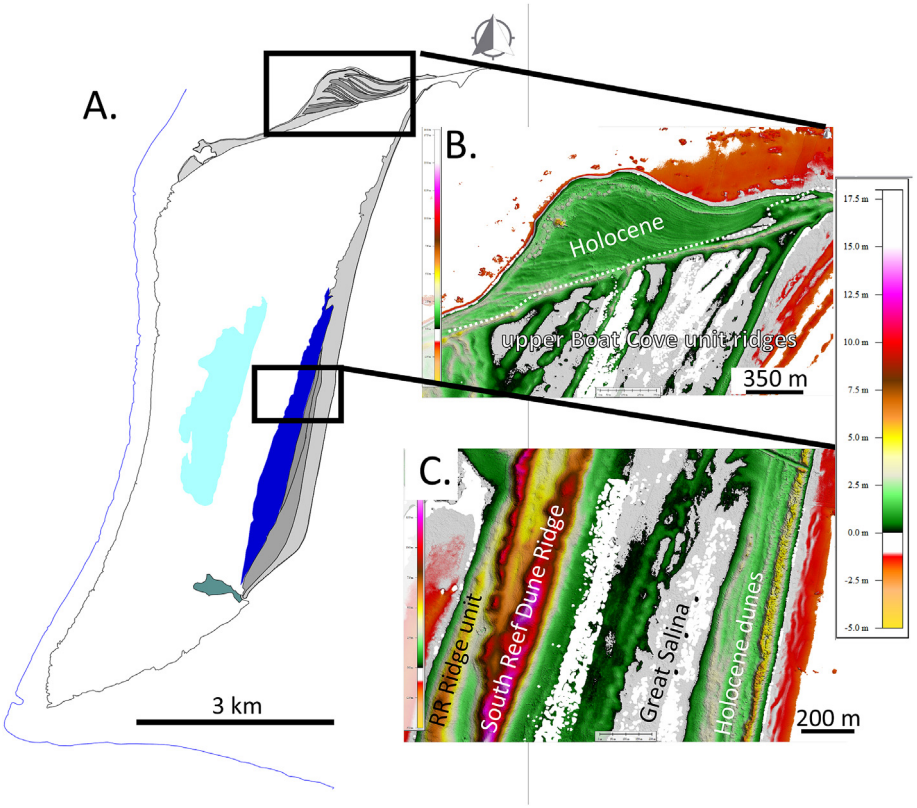

Fig. 26. (a) Holocene depositional elements of West Caicos (gray) with Holocene lacustrine (light blue) and salina (dark blue) elements. (b) Lidar image of northern strandplain complex that averages less than 1 m in elevation and is made of numerous meter-scale linear ridges prograding into sediment supply to the east. (c) Lidar image of eastern ridge system has dune heights up to 6 m and is ornamented by active or semi-active dunes with a prevailing north–south transport direction.

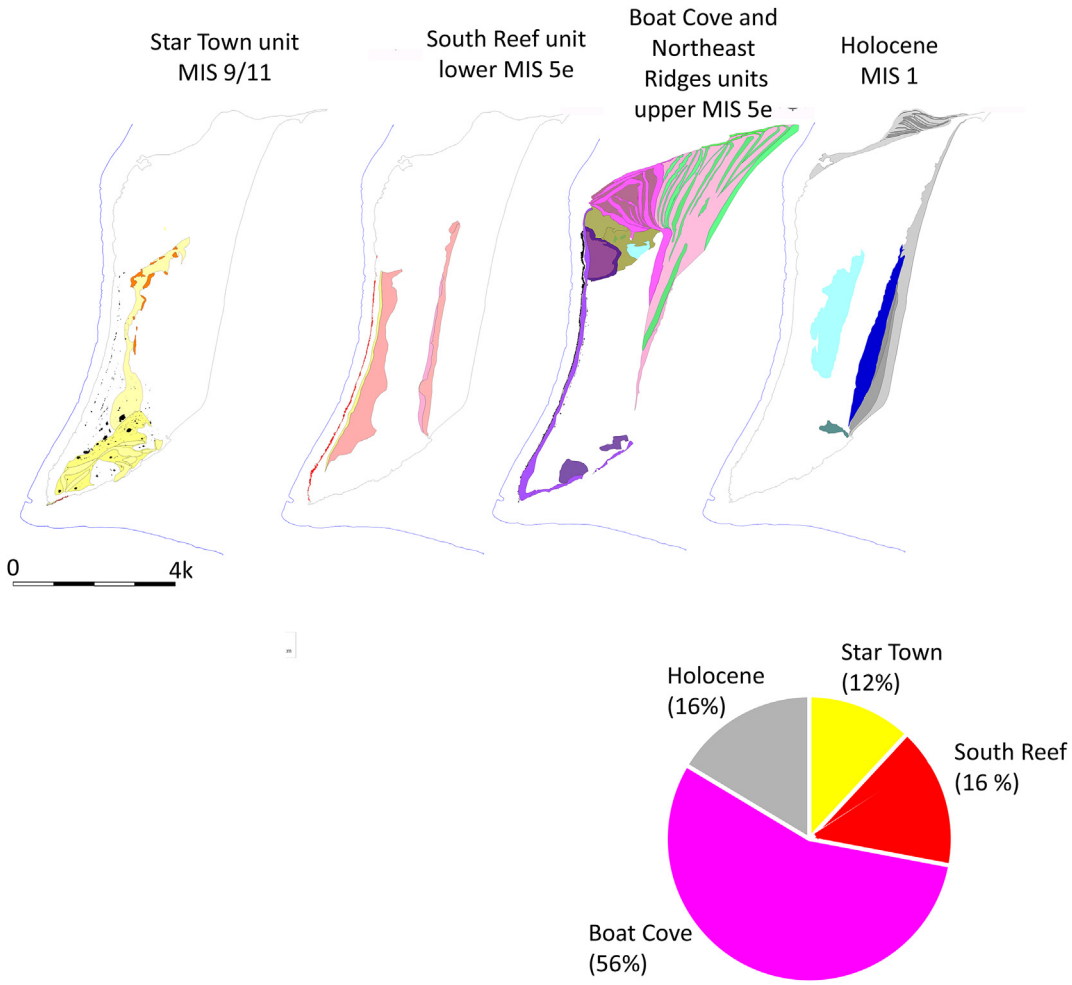

Fig. 27. Subdivision of West Caicos into relative stratigraphic units and estimation of land surface area occupied by each unit. Pie chart shows percentage of surface area representing each interglacial. The previously unmapped middle Pleistocene Star Town MIS 9/11 unit makes up 12 percent of island, whereas dominant depositional event is the upper MIS 5e, which accounts aerially for more than half the accretionary record of the island.

(Kopp et al., 2013) the authors conclude that an intra-LIG sea level fall followed by a rise, with a total differential in excess of 4 m, is extremely likely. This intra-MIS 5e fall is also recorded by the Lisiecki and Raymo (2005) stacked $\delta^{18}O$ composite curve that illustrates an intra-5e drop in values equating to a small-scale short-lived sea-level fall (Fig. 3A).

The Bahamas and Caribbean show abundant evidence for an intra-MIS 5e unconformity (Neumann and Hearty, 1996; Hearty et al., 2007), most notably from the Devil's Point area on Great Inagua (White et al., 1998; Wilson et al., 1998; Thompson and Goldstein, 2005; Thompson et al., 2011; Skrivanek et al., 2018), with a lesser signal in the Cockburn Town reef (Hearty and Kindler, 1993; White et al., 1998; Wilson et al., 1998; Skrivanek et al., 2018). The detailed U–Th dating by Thompson et al. (2011) on Great Inagua proposes the two intra-5e sea-level peaks to occur at 123 ka at approximately +4 m and 119 ka at approximately +6 m. The intra-5e unconformity that splits these two highstands would be bracketed by these dates, agreeing reasonably well with the chronology proposed here (126.5 ka and 120.6 ka) and by Hearty et al. (2007).

A complex intra-5e history has also been documented from cores in the Red Sea (Rohling et al., 2008) as well as in outcrops showing stacked unconformity-bound reef successions around the Red Sea. The work of both Plaziat et al. (1995) and Bruggemann et al. (2004) documents distinct unconformities driven, at least in the case of Plaziat et al. (1995), by an unequivocal downward shift in coastal onlap that dictates a sea-level-fall origin. Several sites on the coast of Western Australia (O'Leary et al., 2013) have also provided clear evidence of a dual-pulsed sea level change record for the LIG, with an initial glacio-isostatic adjustment (GIA)-corrected rise to +3.4 m followed by a relative fall and accompanying erosion, and finally a second greater rise to +9 m. In the Mediterranean, Hearty (1986, 1987) initially proposed a complex intra-MIS 5e record that has later been further established by a range of detailed studies (e.g., Carboni et al., 2014, and reviews of interpretations therein). Carboni et al. (2014) refer to a minor and compound initial rise in the early MIS 5e to +3 m at approximately 127 ka, followed by a fall to present-day sea level and a second rise to +5.5 m peaking near 126 ka.

Detailed study of the MIS 5e reefs at Xcaret on the Yucatan coast south of Playa del Carmen (Blanchon et al., 2009) proposes a two-phase MIS 5e history with an initial rise to +3 m at approximately 134–132 ka, followed by drowning and back-stepping of the lower reef and establishment of a younger 119–117 ka reef system at +6 m. In the Florida Keys, the extensive mapping and dating summarized by Muhs et al. (2011) seem to only record the younger phase of reef growth (given as 120 ka) reaching an estimated sea-level elevation of +6 m.

Taken globally, there is strong evidence for a two-phase depositional history of the MIS 5e, as has been noted by the majority of the authors cited above. The main uncertainty in the data sets is the nature of the intra-MIS 5e perturbation. We feel the data along the west coast of West Caicos present by far the strongest stratigraphic and sedimentological evidence for a brief sea-level-fall event that drove substantial erosional modification of the early (127 ka) MIS 5e reefal platform. There is no question that the stratigraphic response of the various BTC islands to this event is variable, and that this variability might be in large part a reflection of differences in glacio-isostatic adjustments. Regardless, a clear documentation of this major and here unambiguous intra-MIS 5e unconformity needs to be presented and considered as a part of the larger global sea level record.

6.3. *Patterns of island accretion, sea-level changes, and subsidence during the last half-million years*

The focus of studies by Wanless and Dravis (1989), Jones and Awiller (2008), and Simo et al. (2008) has been in large part on understanding Holocene/Pleistocene facies patterns as they might shed light on the interpretation of older and less-well-controlled depositional systems in other parts of the Phanerozoic. By integrating detailed understanding of interglacial eustatic signals and stratigraphic frameworks generated for Bahamian platforms by previous workers (Garrett and Gould, 1984; Vacher et al., 1989; Carew and Mylroie, 1995; Hearty and Kindler, 1993, 1995; Hearty, 1998) with the study of West Caicos using detailed mapping enhanced by UAV and lidar imagery, it has been possible to derive a more complete history of island evolution than previously recognized (Fig. 27).

The Pleistocene history of West Caicos begins with flooding and deposition of the Star Town unit during MIS 9/11. Subtidal, foreshore, and eolian strata with minor reef development in the northwest created the nucleus of the island of West Caicos with a southern shoreline that has remained pinned approximately in place while accretion occurred to the north and east and, to a lesser extent, west during later interglacials (Fig. 14A). Following a prolonged period of exposure and karstification (330–132 ka), initial MIS 5e transgression and development of the South Reef complex occurred between 132 and 125 ka at +3.5–4 m sea-level elevation along the west coast of the island while beach–dune ridge complexes were deposited along the east coast. A brief fall to an estimated +0.5 m above present, or possibly just below, at approximately 120 ka is interpreted from the significant erosional downcutting and deposition of a coarse coral–lithoclast conglomerate. A second sea-level rise to a minimum +4.5 m and development of an ooid grainstone dune ridge–strandplain complex dominated accretion on the north and northeast portions of the island, accounting for 57 percent of the surface area (120–116 ka). Forced regressive downstepping as accretion of ooid sands continued is shown by the formation of strandplain deposits below present-day sea-level (116 ka?). Subaerial exposure and formation of a well-developed paleosol/calcrete followed, with some karst modification. Holocene flooding has not been closely constrained, but C^{14} age dates (Lloyd et al., 1987) indicate ooid dune and strandplain deposition had resumed and built the northern and eastern margins of the island outward starting at 3450 ybp (Fig. 26).

7. Summary and conclusions

Pleistocene carbonate islands provide some of the most detailed geologic records of relative sea-level change over perhaps the past half-million years. In particular, the carbonate islands of the western Northern Atlantic (Bahamas, Turks and Caicos, and related islands of the West Indies) display a strikingly consistent stratigraphic record of sea-level change with little variance associated with differential subsidence/uplift. Many of these island stratigraphic records now include middle Pleistocene (MIS 9 or 11), variable presence of MIS 7, and upper and lower MIS 5e, 5a (again depending on the setting of the island), as well as Holocene units. Continued refinement in the positioning of shoreline positions and elevations of interglacial sea stands is critical for providing a more robust understanding of glacioeustacy as well as of the regional tectonic overprints of the eustatic signal.

Detailed geologic mapping of the island of West Caicos on the southwest corner of the Caicos Platform in the British West Indies, was carried out through a combination of techniques. Detailed geologic mapping, high-resolution airborne lidar, and UAV-generated orthophoto-based DEMs reveal a complex anatomy and evolution showing that the island of West Caicos can play a central role in the construction of a Bahamian–Caribbean regional stratigraphic framework. West Caicos is a product of deposition and erosion during the three main interglacial highstands (MIS 9/11 [Star Town unit], both early and late MIS 5e [South Reef, Boat Cove, and Northeast Ridges units], and Holocene MIS 1 [Long Road unit]). Unlike more Atlantic Ocean–exposed islands, apparently deposits of MIS 7 and 5a are not preserved on the island, presumably because of a lower energy threshold.

The western coast of West Caicos consists of a spectacular 8.4-km exposure that contains middle Pleistocene (MIS 9/11), lower and upper MIS stage 5e units, and minor Holocene strata. The island core consists of both marine and eolian facies with a mid-Pleistocene shoreline position of +1 m. Most notably, we document what we believe to be thus far the most detailed record of the intra-MIS 5e unconformity in the western North Atlantic. The early MIS 5e is seen as a fully accreted fringing reef with possible barrier-reef extension, with an *Acropora palmata* reef core and coralline algal crestal facies that reaches to 4 m above present-day sea level (Fig. 17), allowing an estimate of approximately this height for the early MIS 5e sea level at 126.5 ka. The intra-MIS 5e unconformity, mapped for over 5 km of shoreline exposure, is marked by truncation of as much as 3 m of the lower MIS 5e South Reef unit that testifies for a MIS 5e sea-level drop estimated to have been approximately 3–4 m in magnitude, bringing sea-level position down from +4 m to +1 m or lower on the basis of the basal level of erosion. The subsequent late MIS 5e rise, which is the event marking maximum instability and highest rates of sea level rise (Kopp et al., 2013; O'Leary et al., 2013; Hearty and Tormey, 2017) is recorded by a +5-m uppermost foreshore. Unabraded coral heads colonize the top–South Reef erosion surface and are dated at 120.6 ka. Following this high sea level at the close of the interglacial, sea-level fell as shown by a series of progressively downstepping shorelines, referred to here as the *Northeast Ridges unit*, that drove rapid out-building of the north and northeast margins of West Caicos.

Superimposed on this complex sea-level history and island accretion pattern is the growing awareness of an increased sediment accumulation rate tied to the upper MIS 5e interval. The detailed areal mapping of MIS 5e ridges and their lidar-constrained surface topography allows estimation of a 23–38% increase in sediment accumulation rate relative to the MIS 1 (Holocene). This difference in rate between MIS 1 and upper MIS 5e should to be considered a minimum in that it does not consider surface denudation since deposition of the 120 + ka age of the upper MIS 5e. Another important aspect of this upper MIS 5e unit is the shift to a dominantly chemically precipitated grain type (ooid grainstones) as has been noted by several authors. This combination of an increased rate of accumulation and change to dominantly chemically precipitated grains (oolitic-peloidal grainstones) suggests changes

in the larger depositional system that includes a higher sea-level position, but may also reflect a significant change in ocean chemistry and/or temperature.

For stratigraphers trying to unravel the complex record of deposition associated with Milankovitch forcing, it is critical to appreciate that distinct stratigraphic detail in units such as the intra– MIS 5e unconformity on West Caicos can result from eustatic events not tied to solar insolation and precession. Further, for scientists trying to gain an appreciation for the degree of systematic versus chaotic response of sea-level change to climate change, this stratigraphic record is a clear signal that not all events in the recent past can be linked to predictable climate shifts of longer duration. Even casual observation of the complexity of the stable isotope record of the last several interglacials clearly illustrates the potential for non-Milankovitch mechanisms. If only some of these perturbations are real eustatic events, a significant shading of our grasp of glacioeustacy is created.

Acknowledgements

We wish to acknowledge the financial support of the Bureau of Economic Geology's Reservoir Characterization Research Lab sponsors, as well as funding from the Robert K. Goldhammer Endowed Chair in Carbonate Geology at the UT Austin Department of Geological Sciences. Permission to conduct research on the island of West Caicos was provided by the Department of Environment and Maritime Affairs. Dr. Harry Rowe has provided substantial input in selection and geochemical analysis of coral material for the U/Th work. Special thanks to Eric Salamanca of DEMA as well as to DEMA for their support and cooperation. Logistical support on West Caicos was graciously supplied by Apex Development Company, Ryan Blain, Alex Freirs, and Brian Swann. Mark Parrish and Big Blue Unlimited provided critical logistical support. Technical editing by Stephaine Jones of the University of Texas Bureau of Economic Geology greatly clarified the text. Constructive critiques by the editor (Ingrid Hendy), P. Kindler, J. Reijmer, and an anonymous reviewer have significantly improved the manuscript.

Appendix A. Supplementary data

Supplementary data to this article can be found online at https://doi.org/10.1016/j.quascirev.2018.12.010.

References

Adey, W., 1978. Coral reef morphogenesis: a multidimensional model; new data from coring and carbon 14 dating provide keys for unraveling some classical enigmas. Science 202, 831–837.

Blanchon, P., Eisenhauer, A., Fietzke, J., Liebetrau, V., 2009. Rapid sea-level rise and reef backstepping at the close of the last interglacial highstand. Nature 458, 881–884.

Bruggemann, J.H., Buffler, R.T., Mireille, M.M., Guillaume, M.M., Walter, R.C., von Cosel, R., Berhane, N., Ghebretensae, N., Berhe, S.M., 2004. Stratigraphy, paleoenvironments and model for the deposition of the Abdur Reef limestone: context for an important archaeological site from the last interglacial on the Red Sea coast of Eritrea. Palaeogeography, Paleoclimatology, Palaeoecology 203, 179–206.

Carboni, S., Lecca, L., Hillaire-Marcel, C., Ghaleb, B., 2014. MIS 5e at San Giovanni di Sinis (Sardinia, Italy): stratigraphy, U/Th dating, and "eustatic" inferences. Quat. Int. 328–329, 21–30.

Carew, J.L., Mylroie, J.E., 1985. The Pleistocene and Holocene stratigraphy of san salvador island, Bahamas, with reference to marine and terrestrial lithofacies at French Bay. In: Curran, H.A. (Ed.), Pleistocene and Holocene Carbonate Environments on San Salvador Island, Bahamas: Geological Society of America, Orlando, Annual Meeting Field Trip Guidebook: Ft. CCFL Bahamian Field Station, Lauderdale, Florida, pp. 11–61.

Carew, J.L., Mylroie, J.E., 1995. Depositional model and stratigraphy for the quaternary geology of the bahama islands. In: Curran, H.A., Whjite, B. (Eds.), Terrestrial and Shallow Marine Geology of the Bahamas and Bermuda, vol. 300. Geological Society of America Special Paper, pp. 5–32.

Chen, J.H., Curran, H.A., White, B., Wasserburg, G.J., 1991. Precise chronology of the last interglacial period; 234U–230Th data from fossil coral reefs in the Bahamas. Geol. Soc. Am. Bull. 89, 356–368.

Cheng, H., Edwards, R.L., Shen, C.C., Polyak, V.J., 2013. Improvements in 230Th dating, 230Th and 234U half-life values, and U–Th isotopic measurements by multi-collector inductively coupled plasma mass spectrometry. Earth Planet. Sci. Lett. 371, 82–91.

Danger, N., 2016. Formation and evolution of Pleistocene (MIS 5e) strandplain grainstones along the leeward margin of West Caicos Island, BWI. MSc thesis. The University of Texas at Austin, p. 69.

Dravis, Jefferey J., Wanless, Harold R., 2008. Caicos platform models of Quaternary carbonate deposition controlled by stronger easterly trade winds – applications to petroleum exploration. In: SEPM Core Workshop No. 22, Developing Models and Analogs for Isolated Carbonate Platforms- Holocene and Pleistocene of Caicos Platform, British West Indies, pp. 21–27.

Edwards, R.L., Chen, J.H., Wasserburg, G.J., 1987. 238U-234U-230Th-232Th systematics and the precise measurement of time over the past 500,000 years. Earth Planet. Sci. Lett. 81, 175–192.

Freeman-Lynde, R.P., Ryan, W.B.F., 1985. Erosional modification of bahama escarpment. Geol. Soc. Am. Bull. 96, 481–494.

Garrett, P., Gould, S.J., 1984. Geology of new providence island, Bahamas. Geol. Soc. Am. Bull. 95, 209–220.

Godefroid, F., 2012. Géologie de Mayaguana, SE de l'archipel des Bahamas. Terre and Environment 108, 230.

Godefroid, F., Kindler, P., 2016. Prominent geological features of Crooked Island, SE Bahamas. In: Glumac, Bosiljka, Savarese, Michael (Eds.), Proceedings of the 16th Symposium on the Geology of the Bahamas and Other Carbonate Regions. Gerace Research Center, pp. 26–38.

Guidry, S.A., Grasmueck, M., Carpenter, D.G., Gombos Jr., A.M., Bachtel, S.L., Viggiano, D.A., 2007. Karst and early fracture networks in carbonates, Turks and Caicos islands, British West Indies. J. Sediment. Res. 77, 508–524.

Haugerud, R.A., Harding, D.J., 2001. Some algorithms for virtual deforestation (VDF) of lidar topographic survey data. International Archives of Photogrammetry and Remote Sensing XXXIV-3/W4, 211–217.

Hearty, P.J., 1986. An inventory of Last Interglacial (sl.) age deposits from the Mediterranean basin: a study in isoleucine epimerization and U/Th dating. Zeitschrift fur Geomorphologie, Supplement Band 62, 51–69.

Hearty, P.J., 1987. New data on the Pleistocene of mallorca. Quat. Sci. Rev. 6, 245–257.

Hearty, P.J., 1998. The geology of Eleuthera island, Bahamas: a rosetta stone of quaternary stratigraphy and sea-level history. Quat. Sci. Rev. 17, 333–355. https://doi.org/10.1016/S0277-3791(98)00046-8.

Hearty, P.J., 2002. Revision of the late Pleistocene stratigraphy of Bermuda. Sediment. Geol. 153, 1–21.

Hearty, P.J., Dai Pra, G., 1992. The age and stratigraphy of middle Pleistocene and younger deposits along the Gulf of Taranto (Southeast Italy). J. Coast Res. 8, 882–905.

Hearty, P.J., Kaufman, D.S., 2000. Whole-rock aminostratigraphy and Quaternary sea-level history of the Bahamas. Quat. Res. 54, 163–173.

Hearty, P.J., Kaufman, D.S., 2009. A high-resolution chronostratigraphy for the central Bahama Islands based on AMS 14C ages and amino acid ratios in whole-rock and *Cerion* land snails. Quat. Geochronol. 4, 148–159.

Hearty, P.J., Kindler, P., 1993. New perspectives on Bahamian geology: san salvador island, Bahamas. J. Coast Res. 9, 577–594.

Hearty, P.J., Kindler, P., 1995. Sea-level highstand chronology from stable carbonate platforms (Bermuda and the Bahamas). J. Coast Res. 11, 675–689.

Hearty, P.J., Kindler, P., 1997. The stratigraphy and surficial geology of New Providence and surrounding islands, Bahamas. J. Coast Res. 13, 798–812.

Hearty, P.J., Tormey, B.R., 2017. Sea-level change and superstorms; geologic evidence from late last interglacial (MIS 5e) in Bahamas and Bermuda offers ominous prospects for a warming Earth. Mar. Geol. 390, 347–365. https://doi.org/10.1016/j.margeo.2017.05.009.

Hearty, P.J., Vacher, H.L., 1994. Quaternary stratigraphy of Bermuda: a high-resolution pre-Sangamonian rock record. Quat. Sci. Rev. 13, 685–697.

Hearty, P.J., O'Leary, M.J., Kaufman, D.S., Page, M., Bright, J., 2004. Amino acid geochronology of individual foraminifer (*Pulleniatina obliquiloculata*) tests, north Queensland margin, Australia: a new approach to correlating and dating Quaternary tropical marine sediment cores. Paleoceanography 19, PA4022. https://doi.org/10.1029/2004PA001059.

Hearty, P.J., O'Leary, M.J., Donald, A., Lachlan, T., 2006. The enigma of 3400 yr BP coastal oolites in Tropical northwest Western Australia…why then, why there? Sediment. Geol. 186, 171–185.

Hearty, P.J., Hollin, J.T., Neumann, A.C., O'Leary, M.J., McCulloch, M., 2007. Global sea-level fluctuations during the Last Interglaciation (MIS 5e). Quat. Sci. Rev. 26, 2090–2112.

Jackson, K.L., Eberli, G.P., Reid, S.B., McNeill, D.F., Harris, P.M., Klaus, J.S., 2012. Evidence and amplitude of sea-level oscillations during the Last Interglacial Highstand (MIS 5e) from the Bahamas. Geological Society of America Abstracts with Programs 44 (7), 54.

Jones, G.D., Awiller, D.N., 2008. Depositional porosity and permeability calculated from modern carbonate sediments, Turks and Caicos Islands. British West Indies: SEPM Core Workshop 22, 147–159.

Kaufman, D.S., 2003. Amino acid paleothermometry of quaternary ostracodes from the bonneville basin, Utah. Quat. Sci. Rev. 22, 899–914.

Kaufman, D.S., 2006. Temperature sensitivity of aspartic and glutamic acid racemization in the foraminifera *Pulleniatina*. Quat. Geochronol. 1, 188–207.
Kaufman, D.S., Manley, W.F., 1998. A new procedure for determining entaiomeric (D/L) amino acid ratios in fossil using reverse phase liquid chromatography. Quat. Sci. Rev. 17, 987–1000.
Kindler, P., 1995. New Data on the Holocene Stratigraphy of Lee Stocking Island: Terrestrial and Shallow Marine Geology of the Bahamas and Bermuda, vol. 300. Geological Society of America special publication, p. 105.
Kindler, P., Hearty, P.J., 1995. Pre-sangamonian eolianites in the Bahamas? New evidence from Eleuthera island. Mar. Geol. 127, 73–86.
Kindler, P., Hearty, P.J., 1996. Carbonate petrography as an indicator of climate and sea-level changes: new data from Bahamian Quaternary units. Sedimentology 43, 381–399.
Kindler, P., Hearty, P.J., 1997. Geology of the Bahamas: architecture of Bahamian islands. In: Vacher, H.L., Quinn, T. (Eds.), Geology and Hydrogeology of Carbonate Islands., Developments in Sedimentology, vol. 54, pp. 141–160.
Kindler, P., Hine, Albert C., 2009. The paradoxical occurrence of oolitic limestone on the eastern islands of Great Bahama Bank: where do the ooids come from? Int. Assoc. Sedimentol. Spec. Pub. 41, 113–122.
Kindler, P., Meyer, A., 2012. New U/Th and amino-acid racemization dating and interpretation of Pleistocene sequences from West Caicos Island (Caicos platform): implication for cyclostratigraphy. In: Proceedings of the 15th Symposium on the Geology of the Bahamas and Other Carbonate Regions, pp. 82–95.
Kindler, P., Reyss, J.-L., Cazala, C., Plagnes, V., 2007. Discovery of a composite reefal terrace of middle and late Pleistocene age in Great Inagua Island, Bahamas: implications for regional tectonics and sea-level history. Sediment. Geol. 141–147.
Kindler, P., Godefroid, F., Chiaradia, M., Ehlert, C., Eisenhauer, A., Frank, M., Hasler, C.A., Samankassou, E., 2011. Discovery of Miocene to early Pleistocene deposits on Mayaguana, Bahamas: evidence for recent active tectonism on the North American margin. Geology 39, 523–526. https://doi.org/10.1130/G32011.1.
Kopp, R.E., Simons, F.J., Mitrovica, J.X., Maloof, A.C., 2009. Probabilistic assessment of sea level during the last interglacial stage. Nature 462, 863–867.
Kopp, Robert E., Simons, Frederik J., Mitrovica, Jerry X., Maloof, Adam C., Oppenheimer, Michael, 2013. A probabilistic assessment of sea level variations within the last interglacial stage: Geophys. J. Int. v. 193, 711–716.
Kraus, K., Pfeifer, N., 1998. Determination of terrain models in wooded areas with airborne laser scanner data. ISPRS J. Photogrammetry Remote Sens. 53, 193–203.
Lisiecki, L.E., Raymo, M.E., 2005. A Pliocene-Pleistocene stack of 57 globally distributed benthic δ18O records. Paleoceanography 20, 17. https://doi.org/10.1029/2004PA001071.
Lloyd, R., Perkins, R., Kerr, S., 1987. Beach and shoreface ooid deposition on shallow interior banks, Turks and Caicos Islands, British West Indies. J. Sediment. Res. 57, 976–982.
Lynts, G.W., 1970. Conceptual model of the Bahamian Platform for the last 135 million years. Nature 225, 1226–1228.
Morgan, W.A., 2008. Holocene sediments of northern and western Caicos platform, British West Indies. In: Morgan, W.A., Harris, P.M. (Eds.), Workshop on Developing Models and Analogs for Isolated Carbonate Platforms—holocene and Pleistocene Carbonates of Caicos Platform, British West Indies. SEPM Short Course, pp. 75–104.
Muhs, D.R., Simmons, K.R., Randall Schuman, R., Halley, R.B., 2011. Sea-level history of the past two interglacial periods: new evidence from U-series dating of reef corals from south Florida. Quat. Sci. Rev. 30, 570–590.
Mullins, Henry T., Hine, Albert C., 1989. Scalloped bank margins: beginning of the end for carbonate platforms? Geology 17, 30–33.
Mullins, H.T., Lynts, G.W., 1977. Origin of the northwestern Bahama Platform: review and reinterpretation. Geol. Soc. Am. Bull. 88, 1447–1461.
Murray-Wallace, C.V., 2018. Quaternary History of the Coroong Coast Plain, Southern Australia: an Archive of Environmental and Global Sea-level Change. Springer, p. 275.
Neuman, C.J., Cry, G.W., Caso, E.L., Jarvien, B.R., 1978. Tropical Cyclones of the North Atlantic Ocean, 1871–1977: National Climatic Center. U.S. Govt. Printing Office, Asheville, N. C., p. 170. Stock #003-17-00425-2.
Neumann, A.C., Hearty, P.J., 1996. Rapid sea-level changes at the close of the last interglacial (substage 5e) recorded in Bahamian island geology. Geology 24, 775–778.
O'Leary, M., Hearty, P.J., Thompson, W.G., Raymo, M.E., Mitrovica, J.X., 2013. Ice sheet collapse following a prolonged period of stable sea level during the last interglacial. Nat. Geosci. 6, 796–800.
Plaziat, J.-C., Baltzer, F., Choukri, A., Conchon, O., Freytet, P., Orzag-Sperber, F., Purser, B., Raguideau, A., Reyss, J.-L., 1995. Quaternary changes in the Egyptian shoreline of the northwestern Red Sea and gulf of suez. Quat. Int. 29/30, 11–22.
Rankey, E.C., Guidry, S.A., Reeder, S.L., Guarin, H., 2009. Geomorphic and sedimentologic heterogeneity along a Holocene shelf margin: Caicos Platform. J. Sediment. Res. 79, 440–456.
Read, J.F., 1999. In: Phanerozoic Carbonate Ramps from Greenhouse, Transitional and Ice-house Worlds: Clues from Field and Modelling Studies, vol. 149. Geological Society of London Special Publication, pp. 107–135.
Rohling, E.J., Grant, K., Hemleben, Ch, Siddall, M., Hoogakker, B.A.A., Bolshaw, M., Kucera, M., 2008. High rates of sea-level rise during the last interglacial period. Nat. Geosci. 1, 38–42.
Rowe, M., Bristow, C., 2015. Sea-level controls on carbonate beaches and coastal dunes (eolianite): lessons from Pleistocene Bermuda. Geol. Soc. Am. Bull. 127, 1645–1665.
Shackleton, N.J., 2000. The 100,000-year ice-age cycle identified and found to lag temperature, carbon dioxide, and orbital eccentricity. Science 289, 1897–1902.
Sherman, C.E., Fletcher, C.H., Rubin, K.H., Simmons, K.R., Adey, W.H., 2014. Sea-level and reef accretion history of Marine Isotope Stage 7 and late Stage 5 based on age and facies of submerged late Pleistocene reefs. Oahu, Hawaii, Quaternary Research 81, 138–150.
Simo, J.T., Guidry, S.A., Iannello, C., Rankey, E.C., Harris, C.E., Guarin, H., Ruf, A., Hughes, T., Derewetzka, A.N., Parker, R.S., 2008. Holocene-pleistocene geology of a transect of from isolated carbonate platform, NW Caicos platform, British West Indies. SEPM Core Workshop 22, 111–118.
Skrivanek, Alexandra, Li, Jin, Dutton, Andrea, 2018. Relative sea-level change during the Last Interglacial as recorded in Bahamian fossil reefs. Quat. Sci. Rev. 200, 160–177.
Thompson, W.G., Goldstein, S.L., 2005. Open-system coral ages reveal persistent suborbital sea-level cycles. Science 308, 401–404.
Thompson, W.G., Curran, H.A., Wilson, M.A., White, B., 2011. Sea-level oscillations during the last interglacial highstand recorded by Bahamas corals. Nat. Geosci. 4, 684–687. https://doi.org/10.1038/NGEO1253.
Turner, D., Lucieer, A., Watson, C., 2012. An automated technique for generating georectified mosaics from ultra-high resolution unmanned aerial vehicle (UAV) imagery, based on structure from motion (SfM) point clouds. Rem. Sens. 4, 1392–1410.
Vacher, H.L., 1973. Coastal dunes of younger Bermuda. In: Coates, D.R. (Ed.), Coastal Geomorphology. Publications in Geomorphology. State University of New York, Binghamton, pp. 355–391.
Vacher, H.L., Quinn, T., 1997. Geology and hydrogeology of carbonate islands. Dev. Sedimentol. 54, 35–90.
Vacher, H.L., Rowe, M., Garrett, P., 1989. Geologic Map of Bermuda. Oxford Cartographers, U.K, 1:25,000 scale.
Waelbroeck, C., Labeyrie, L., Michel, E., Duplessy, J.C., McManus, J., Lambeck, K., Balbon, E., Labracherie, M., 2002. Sea-level and deep water temperature changes derived from benthic foraminifera isotopic records. Quat. Sci. Rev. 21, 295–305.
Waltz, M.D., 1988. The Evolution of Shallowing-upwards Reef to Oolite Sequences at the Leeward Margin of Caicos Platform, BWI. M.S. thesis. University of Miami, p. 95.
Wanless, H., Dravis, J., 1989. Carbonate environments and sequences of Caicos platform. Field Trip Guide Bk. 374, 75.
Wanless, H.R., Tedesco, L.P., Tyrell, K.M., 1988. Production of subtidal tubular and surficial tempestites by hurricane kate, Caicos platform, British West Indies. J. Sediment. Petrol. 58, 739–750.
Westoby, M.J., Brasington, J., Glasser, N.F., Hambrey, M.J., Reynolds, J.M., 2012. Structure-from-motion photogrammetry: a low-cost, effective tool for geoscience application. Geomorphology 179, 300–314.
Whitacre, K., Kaufman, D.S., Kosnik, M.A., Hearty, P.J., 2017. Converting A/I values (ion exchange) to D/L values (reverse phase) for amino acid geochronology. Quat. Geochronol. 37, 1–6.
Whitaker, F.F., Smart, P.L., 2004. Chapter 4: hydrogeology of the Bahamian archipelago. Dev. Sedimentol. 54, 183–216.
White, B., Curran, H.A., Wilson, M.A., 1998. Bahamian coral reefs yield evidence of a brief sea-level lowstand during the Last Interglacial. Carbonates Evaporites 13, 10–22.
Wilson, M.A., Curran, H.A., White, B., 1998. Paleontological evidence of a brief global sea-level event during the last interglacial. Lethia 31, 241–250.
Zahm, C., Lambert, J., Kerans, C., 2016. Use of unmanned aerial vehicles (UAVs) to create digital outcrop models: an example from the Cretaceous Cow Creek Formation, Central Texas. GCAGS Journal 5, 180–188.